Climate-change versus landslide origin of fill terraces in a rapidly eroding bedrock landscape: San Gabriel River, California

Dirk Scherler[1,2,3,†], Michael P. Lamb[1], Edward J. Rhodes[4,5], and Jean-Philippe Avouac[1]
[1]*Division of Geological and Planetary Sciences, California Institute of Technology, 1200 East California Boulevard, Pasadena, California 91125, USA*
[2]*GFZ German Research Centre for Geosciences, 14473 Potsdam, Germany*
[3]*Institute of Geological Sciences, Freie Universität Berlin, Malteserstrasse 74-100, 12249 Berlin, Germany*
[4]*Department of Geography, University of Sheffield, Winter Street, Sheffield, S10 2TN, UK*
[5]*Department of Earth, Planetary, and Space Sciences, University of California–Los Angeles, 595 Charles Young Drive East, Los Angeles, California 90095, USA*

ABSTRACT

Fill terraces along rivers represent the legacy of aggradation periods that are most commonly attributed to climate change. In the North Fork of the San Gabriel River, an arid bedrock landscape in the San Gabriel Mountains, California, a series of prominent fill terraces was previously related to climate-change–induced pulses of hillslope sediment supply that temporarily and repeatedly overwhelmed river transport capacity during the Quaternary. Based on field observations, digital topographic analysis, and dating of Quaternary deposits, we suggest instead that valley aggradation was spatially confined to the North Fork San Gabriel Canyon and was a consequence of the sudden supply of unconsolidated material to upstream reaches by one of the largest known landslides in the San Gabriel Mountains. New ^{10}Be-derived surface exposure ages from the landslide deposits, previously assumed to be early to middle Pleistocene in age, indicate at least three Holocene events at ca. 8–9 ka, ca. 4–5 ka, and ca. 0.5–1 ka. The oldest and presumably most extensive landslide predates the valley aggradation period, which is constrained by existing ^{14}C ages and new luminescence ages to ca. 7–8 ka. The spatial distribution, morphology, and sedimentology of the river terraces are consistent with deposition from far-traveling debris flows that originated within, and mined, the landslide deposits. Valley aggradation in the North Fork San Gabriel Canyon therefore resulted from locally enhanced sediment supply that temporarily overwhelmed river transport capacity, but the lack of similar deposits in other parts of the San Gabriel Mountains argues against a regional climatic signal. Our study highlights the potential for valley aggradation by debris flows in arid bedrock landscapes downstream of landslides that occupy headwater areas.

INTRODUCTION

The way in which landscapes respond to climate and other environmental changes is an important issue in light of global climate change and anthropogenic changes in land use (National Research Council, 2010). Most geomorphic research in this direction has so far focused on soil-mantled landscapes and how changes in rainfall, vegetation cover, and runoff lead to changes in sediment transport on hillslopes and by rivers (e.g., Knox, 1983; Blum and Törnqvist, 2000). Far less inquiry has addressed how rapidly eroding, steep bedrock landscapes respond to environmental changes (e.g., Riebe et al., 2001; DiBiase and Lamb, 2013; Scherler et al., 2015). This is a shortcoming, because steep hillslopes and higher mass fluxes have the potential for a greater and more rapid impact on ecosystems and societies. The San Gabriel Mountains in Southern California, for example, rate amongst the most rapidly uplifting mountains in the United States. Their steep slopes and sensitivity to wildfires, flash floods, landslides, and debris flows account for imminent hazards to nearby urban areas (e.g., Eaton, 1935; Lavé and Burbank, 2004; Lamb et al., 2011; Kean et al., 2013). An assessment of the potential risks that are associated with climatic and other environmental changes requires understanding the controls on sediment production and transport in these landscapes and the ways in which they change with time.

Because rates of sediment transport can be quite variable, observational records are often too short to yield reliable trends. This is particularly true in semiarid to arid environments, which are characterized by high rainfall, runoff, and discharge variability (e.g., Molnar et al., 2006). In contrast, aggradational and degradational landforms provide comparatively longer records of landscape change and usually integrate over short-term variability. Amongst the most often used landforms for reconstructing landscape history are river terraces, which are found all across the world. River terraces record the geometry of previous valley floors, which can be used to inform about sea-level variations (e.g., Merritts et al., 1994), or tectonic rates (e.g., Lavé and Avouac, 2001; Pazzaglia and Brandon, 2001). Their formation is most often attributed to landscape-scale effects of climate change (e.g., Leopold et al., 1964; Brakenridge, 1980; Knox, 1983; Weldon, 1986; Bull, 1991; Porter et al., 1992; Poisson and Avouac, 2004; Pazzaglia, 2013; Scherler et al., 2015). However, other studies have shown that terraces can form even during periods of steady downcutting, from intrinsic variations in river lateral migration and meander cutoff (Davis, 1909; Merritts et al., 1994; Finnegan and Dietrich, 2011).

Traditionally, river terraces are subdivided into strath and fill terraces. Whereas strath terraces are cut into bedrock and typically capped with a thin veneer of sediment, fill terraces represent remnants of valley fills that are often several tens to hundreds of meters thick (e.g., Merritts et al., 1994; Pazzaglia, 2013). Most generally, valley fills form when rivers switch from incision to aggradation. In uplifting landscapes that are far away from sea-level changes, aggradation that is due to damming of a river by

†scherler@gfz-potsdam.de

GSA Bulletin; doi: 10.1130/B31356.1; 19 figures; 3 tables; Data Repository item 2016046.

a landslide (e.g., Korup et al., 2006), or glacier (e.g., Montgomery et al., 2004; Scherler et al., 2014), can usually be identified by a distinct spatial association of the fill and the dam. Valley fills that are more regionally distributed are in most cases interpreted as resulting from fluvial aggradation in response to climate change (Bull, 1991).

Whether a river incises, aggrades, or maintains a stable bed, depends on the balance between the river's transport capacity and the supply of sediments from hillslopes (Lane, 1955; Bull, 1979, 1991). Temporal variations in transport capacity are mostly due to changes in discharge and the slope of the bed, whereas both the amount and the caliber of sediment that is supplied from hillslopes may vary. In static equilibrium, rivers neither incise nor aggrade, and their transport capacity is just in balance with the supply of hillslope sediments. Any change of the system's variables may lead to departure from equilibrium. For example, if discharge increases, with everything else staying constant, the river increases its transport capacity and incises. Incision should result in shallowing of the bed gradient until the river reaches a new equilibrium. A decrease in discharge, or an increase in the size or amount of sediment supply, on the other hand, would force a river to aggrade and steepen its bed until shear stresses at the bed become high enough to transport all of its material.

Based on detailed field work and analytical tools available at that time, Bull (1991) suggested that fill terraces in parts of the San Gabriel Mountains in Southern California (Fig. 1) were formed by cycles of river aggradation and incision that occurred in response to temporal variations in hillslope sediment supply and river transport capacity induced by climatic changes. Moreover, Bull (1991) considered the San Gabriel Mountains as a type locality for the response of an unglaciated, semiarid to subhumid mountain range to past climatic changes. Because the San Gabriel Mountains are mostly a steep bedrock landscape (Lamb et al., 2011), rather than a soil-mantled landscape, with slope angles greater than the angle of repose (DiBiase et al., 2012), they are limited in their ability to have a much thicker soil mantle even under different Pleistocene climatic conditions. Because of their apparent significance for understanding how steep bedrock landscapes respond to climate change, we have chosen the San Gabriel Mountains for a detailed analysis using modern analytical tools and the aim to identify the processes responsible for valley aggradation.

STUDY AREA AND PREVIOUS WORK

The San Gabriel Mountains constitute a transpressional basement block adjacent to the Mojave segment of the San Andreas fault (Fig. 1A) that consists of mostly Precambrian igneous and metamorphic rocks as well as Mesozoic granites. It is bounded in the south by the predominantly reverse-slip Sierra Madre–Cucamonga fault zone, along which Holocene uplift rates of ~0.5–0.9 mm yr^{-1} have been inferred, based on offset landforms (Petersen and Wesnousky, 1994; Lindvall and Rubin, 2008). Uplift and exhumation of the San Gabriel Mountains are thought to have initiated at ca. 12 Ma, and accelerated at ca. 5–7 Ma, when the San Andreas fault replaced the San Gabriel fault as the principal strike-slip fault in this region (Matti and Morton, 1993; Blythe et al., 2002). Spatial differences in the onset and rate of uplift between different fault-bounded blocks within the San Gabriel Mountains are thought to be responsible for a northwest-southeast increase in landscape-scale relief that coincides with younger mineral cooling ages (Blythe et al., 2000) and higher ^{10}Be-derived erosion rates (DiBiase et al., 2010), as well as enhanced fluvial erosion and more frequent landsliding (Lavé and Burbank, 2004).

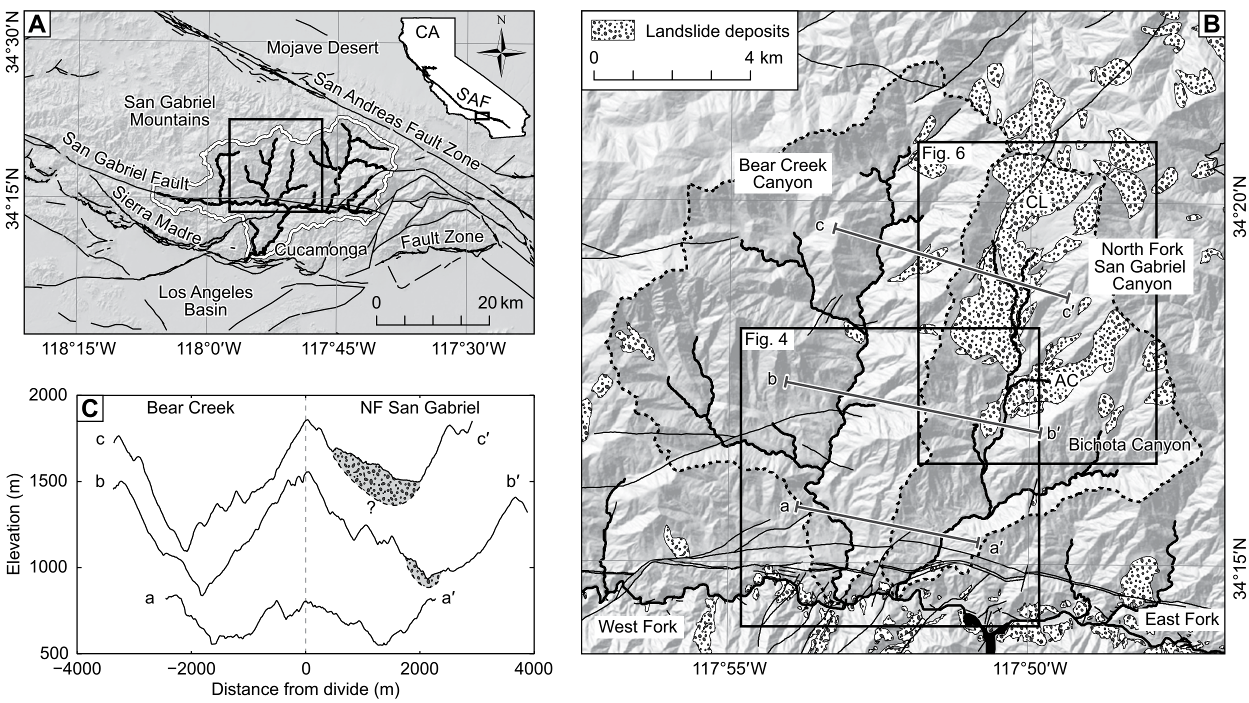

Figure 1. Geographical overview of the study area. (A) Hillshade map of the San Gabriel Mountains in the western Transverse Ranges. Inset shows state of California (CA) with the trace of the San Andreas fault (SAF). (B) Hillshade map of the North Fork San Gabriel and the Bear Creek Canyons. Dotted polygons denote landslide deposits, and thin black lines are faults (Morton and Miller, 2006). (C) Topographic profiles across parts of the Bear Creek and North Fork (NF) San Gabriel Canyons. See B for location.

The largest drainage in the San Gabriel Mountains is the San Gabriel River, with an area of ~580 km^2 (Fig. 1A). Its East and West Forks follow the San Gabriel Valley fault for >40 km, whereas the North Fork of the San Gabriel River is comparatively smaller (49 km^2). Along the lower ~6 km of the North Fork San Gabriel River, Bull (1991) identified four different flights of fill terraces, which he linked to a regional terrace chronology with as many as nine different terrace levels, including sites along the Lytle Creek in the northern San Gabriel Mountains, and the Arroyo Seco in the western San Gabriel Mountains. The relative terrace chronology was substantiated by three Holocene ^{14}C ages from the North Fork San Gabriel Canyon, and by correlation of soil weathering stages (McFadden and Weldon, 1987) and acoustic wave speeds in boulders (Crook, 1986) to dated terraces elsewhere in the western Transverse Ranges. Based on this chronology, Bull (1991) interpreted the fill terraces in the North Fork San Gabriel Canyon to represent four cycles of river aggradation and subsequent incision (i.e., cut-and-fill cycles) that started at around 800, 120, 55, and 6 ka.

The North Fork San Gabriel Canyon stands out against the rest of the San Gabriel Mountains with its abundance of fill terraces (Bull, 1991), at least in the lower part of the catchment. The upper part of the catchment is dominated by two of the largest landslide deposits in the San Gabriel Mountains, the Crystal Lake landslide (CL in Fig. 1B), and the Alpine Canyon (AC in Fig. 1) landslide (Morton et al., 1989). Initial studies (Miller, 1926) interpreted the Crystal Lake landslide as glacial deposits and thus evidence for Pleistocene glaciation in the San Gabriel Mountains. This interpretation was probably related to the fact that the landslide covers a considerable area in the uppermost reaches of the North Fork San Gabriel Canyon. Subsequent studies, however, suggested that the San Gabriel Mountains have not been glaciated during recent glacial periods (Sharp et al., 1959). Given an estimated minimum volume of ~0.6 km^3 (Morton et al., 1989), the Crystal Lake landslide probably involved the collapse of a sizeable mountain flank. The Alpine Canyon landslide is located downstream from the Crystal Lake landslide and is sourced by a small tributary east of the main stem. No dating of either landslide deposit has been undertaken, but the most recent geological map of this area assigns an early to middle Pleistocene age to both landslide deposits (Morton and Miller, 2006).

Adjacent to the North Fork San Gabriel Canyon, there is the somewhat larger (73 km^2) Bear Creek Canyon, which otherwise has a very similar morphology (Fig. 1B). At similar distance from the confluence with the West Fork, the Bear Creek lies ~500 m lower than the North Fork San Gabriel River. This is partly most likely the result of the Crystal Lake landslide deposit (Fig. 1C). The outcropping rocks in both catchments, North Fork San Gabriel and Bear Creek, generally consist of strongly deformed basement rocks, including granitic and gneissic rocks, mylonites, cataclasites, and abundant dikes (Morton and Miller, 2006). Due to their close proximity, and small and similar size, they experience similar climatic conditions and share a similar tectonic and climatic history. If climate change caused fluvial aggradation in the North Fork San Gabriel Canyon, it appears reasonable to expect similar geomorphic responses in the adjacent Bear Creek Canyon. Throughout the remainder of the paper, we will thus repeatedly compare the adjacent North Fork San Gabriel and the Bear Creek Canyons.

The restricted distribution of fill terraces in the San Gabriel Mountains is surprising and atypical for climate change–related fill terraces, which typically are more widely distributed (Knox, 1983). Furthermore, the spatial proximity of terraces and landslides in the North Fork San Gabriel Canyon merits attention not previously granted. Specifically, we ask the question whether this proximity is purely coincidental or related. In the following, we will present field observations, analysis of high-resolution digital topography, and cosmogenic exposure-age and luminescence dating that lead us to consider an alternative mechanism for valley aggradation in the North Fork San Gabriel Canyon and that hold implications for the response of bedrock landscapes to climate change.

DATA AND METHODS

Topographic Analysis and Field Observations

The spatial distribution of terraces and landslide deposits in the North Fork San Gabriel and Bear Creek Canyons was documented by Bull (1991) and Morton and Miller (2006). We complemented existing maps by our own field observations using a handheld global positioning system (GPS), topographic maps, and high-resolution aerial images. Because dense chaparral restricts direct access to most of the landscape, we supplemented our field work with digital elevation model (DEM) analysis using MATLAB® and the TopoToolbox v2 (Schwanghart and Scherler, 2014). The 3-m-resolution DEM is based on interferometry of synthetic aperture radar (IfSAR) data, which were acquired during winter 2002–2003 and provided by the National Oceanic and Atmospheric Administration (NOAA) Coastal Services Center. Comparison with the 10-m-resolution National Elevation Data set indicates that besides the influence of vegetation, the IfSAR-derived DEM has higher errors in steep terrain (>20°).

Our digital mapping of terrace surfaces used automatic identification of potential terrace pixels in the DEM, based on surface gradient, curvature, and proximity to other pixels of similar attributes. Subsequently, we evaluated the results by comparison with manually mapped terrace surfaces in the North Fork San Gabriel Canyon. It has been pointed out that the spatial correlation of individual terraces can be misleading and whenever possible should be substantiated with age dating (Merritts et al., 1994). In our study area, however, distances between individual terraces are short (<1 km), and along-stream extents of some terraces are large (>200 m). These facts allowed us to identify the inclination of terrace surfaces and reconstruct valley bottoms along the stretch of the studied valleys.

Although terrace surfaces ought to represent former valley floors, surface processes modify their morphology after abandonment. In particular, dissection by tributary rivers or colluvial deposition from adjacent hillslopes can modify terrace surfaces and obscure the original valley floor gradient. We are aware that this methodology therefore fails when it comes to heavily degraded terraces such as Bull's (1991) T1 terrace. For comparing terrace surface gradients with the gradients of the adjacent river channels, we projected each terrace pixel into a smooth flow path along the valley and fitted a straight line to the distance-elevation pairs of all DEM pixels that corresponded to a given terrace surface. Although the smoothing of the flow path changed its plan-view shape, we retained for each pixel on the flow path its distance along the river from the unsmoothed flow path. This way, we avoided changes in the length of the flow path (and thus gradient) through the smoothing procedure.

To estimate sediment caliber, we conducted grain-size counts within the present-day river channel, on the floodplain, and along terrace outcrops, based on pace measurements at equal steps of 1 m, without double counts, and recorded the intermediate axis of each grain. We acknowledge, however, that comparison of surface measurements, where sorting of grain sizes can be expected (e.g., Parker and Klingeman, 1982), with those from outcrops is not straightforward. Our expectation is that grain size counts from the modern channel may be biased by larger grains.

TABLE 1. SINGLE-GRAIN K-FELDSPAR POST-IR IRSL AGE ESTIMATES

Sample ID	Lab code	Depth (m)	Elevation (m)	Number of dated grains	Number of dated grains used for age estimate	Dose rate* (mGy yr^{-1})	Equivalent dose* (Gy)	Age* (ka)
SG13-01	J0525	25	576	36	6	3.67 ± 0.23	27.1 ± 2.4	7.4 ± 0.8
SG13-02	J0526	25	576	46	7	3.68 ± 0.23	27.5 ± 2.1	7.5 ± 0.7
SG13-03	J0527	20	571	116	1	3.94 ± 0.35	22.1 ± 4.7	5.6 ± 1.3
SG13-04	J0528	4	813	109	4	4.39 ± 0.27	35.8 ± 4.0	8.2 ± 1.0
SG13-05	J0529	4	813	25	2	4.27 ± 0.25	29.8 ± 7.2	7.0 ± 1.7

Note: IR—infrared; IRSL—infrared-stimulated luminescence.
*Errors reflect 1σ uncertainties.

TABLE 2. ^{10}Be SAMPLE DETAILS AND ANALYTICAL RESULTS

Sample ID	Latitude (°N)	Longitude (°W)	Elevation above sea level (m)	Boulder dimensions Height (m)	Width (m)	Length (m)	Mean sample thickness (cm)	Topographic shielding	^{10}Be concentration*,† (atoms/g Qz)	Exposure age§ (ka)
DS103	34.3157	117.8468	1730	1.7	2.5	3	8	1.000	52,181 ± 1821	4.0 ± 0.4
DS106	34.3153	117.8445	1702	1.9	2.5	3	5	0.998	49,143 ± 1752	3.7 ± 0.3
DS203	34.3055	117.8466	1422	4	4.5	7.5	7.5	0.998	55,599 ± 2586	5.0 ± 0.5
DS206	34.3062	117.8528	1603	1.5	2	2	5.5	0.985	449,291 ± 8980	32.7 ± 2.9
DS303	34.2815	117.8442	928	1.6	2	2	7	1.000	68,496 ± 2225	8.5 ± 0.8
DS304	34.2815	117.8441	930	2	2.8	3	4.5	1.000	64,201 ± 6054	7.7 ± 1.0
DS305	34.2814	117.8440	929	1	1.5	3	3.5	1.000	75,754 ± 3040	9.1 ± 0.9
DS402	34.2900	117.8355	1074	3	2.5	3	3	0.997	6997 ± 868	0.8 ± 0.1
DS403	34.2910	117.8349	1096	1.5	2	2.5	7	1.000	9066 ± 759	1.0 ± 0.1
DS404	34.3066	117.8426	1426	3.5	2.5	3	3	0.998	46,803 ± 2387	4.2 ± 0.4
DS405	34.3065	117.8427	1424	2	2.5	6	7	1.000	43,610 ± 1946	4.0 ± 0.4
DS406	34.3123	117.8369	1536	6	5	6	3.5	0.997	49,394 ± 1491	4.1 ± 0.4
DS502	34.2881	117.8233	1420	3	4	2.5	10	0.908	7661 ± 3283	0.8 ± 0.3
DS503	34.2894	117.8238	1361	1.6	2	2.5	2	0.952	6720 ± 3031	0.6 ± 0.3
DS504	34.2887	117.8257	1377	1	2.4	2.8	10	0.999	7179 ± 3671	0.7 ± 0.3

*The subtracted laboratory process blank ^{10}Be/^{9}Be ratios are 5.5 × 10^{-15} (DS103–DS305) and 3.8 × 10^{-15} (DS402–DS504). The ^{10}Be/^{9}Be ratios were normalized to the ^{10}Be standard 07KNSTD with a nominal ^{10}Be/^{9}Be ratio of 2.85 × 10^{-12} (Nishiizumi et al., 2007).
†^{10}Be concentration uncertainties reflect total analytical uncertainties at 1σ level.
§Exposure ages with external uncertainties based on a time-dependent version (Balco et al., 2008) of the production rate scaling model by Lal (1991) and Stone (2000).

Geochronological Control

Infrared Stimulated Luminescence Dating

To obtain age constraints on the aggradational episode in the North Fork San Gabriel Canyon, we collected five samples for dating by single-grain postinfrared infrared stimulated luminescence (post-IR IRSL) analysis of K-feldspar at two locations. Samples were collected in steel tubes pushed horizontally into sandy units within vertical sediment exposures. In situ gamma spectrometer measurements were made at each sample location, to determine the gamma dose rate contribution from the surrounding sediment. Sediment beta dose rates were based on U, Th, and K concentrations determined using inductively coupled plasma–mass spectrometry (ICP-MS) and optical emission spectrometry (OES), corrected for grain size and water content attenuation. Cosmic dose rates were estimated using present burial depths. The analytical results and calculated ages are provided in Table 1.

The luminescence dating approach adopted here is relatively new, and it is particularly suited for regions where quartz grains display low optically stimulated luminescence (OSL) sensitivity (Rhodes, 2015). A detailed description of the analytical procedures is provided in the supplementary materials[1] and in Rhodes (2015). The specific advantage of measuring single grains is that sediments deposited rapidly, or close to their source, may contain many grains that were exposed to insufficient daylight to fully reset their luminescence signals. The use of single grains allowed us to isolate the grains with the minimum equivalent dose (D_e) values by successively excluding grains with high D_e values until the remaining population was consistent with an overdispersion value of ≤15% (for details, see Rhodes, 2015). The post-IR IRSL signal we used is less rapidly bleached by sunlight than the quartz OSL signal (Rhodes, 2011), and our samples displayed many grains that had very high dose values. The single-grain post-IR IRSL age estimates presented here are based on results from a small proportion of grains with low dose estimates; the results of many other grains with apparently old age estimates were rejected as representing grains that were not exposed to light during, or immediately before, their transport and deposition within the sampled sedimentary unit. In adopting this approach we follow long-established luminescence dating procedures for the interpretation of single-grain results (Roberts et al., 1999). Where we observed no indications of postdepositional sediment disturbance, we rigorously used the minimum dose values to estimate age. In our presentation of the single-grain results, we only show grains with ages younger than 100 ka for clarity, although grains with older, and often saturated, ages were measured too. A single, very young grain, which we interpret as introduced by bioturbation from a nearby burrow encountered during sampling, was excluded from age analysis for sample SG13-04.

[1]GSA Data Repository item 2016046, additional details on the single-grain post-IR IRSL dating, and a color version of Figure 8B, is available at http://www.geosociety.org/pubs/ft2016.htm or by request to editing@geosociety.org.

^{10}Be Exposure Dating

We used *in situ*–produced ^{10}Be surface exposure dating of landslide boulders to constrain the history of landslide occurrence in the North Fork San Gabriel Canyon. In the field, we identified large (>3 m) and presumably stable boulders, i.e., wider than tall and imbedded within the surrounding deposits, which showed no evidence of recent spallation. We took our samples from the top surface of each boulder, and we recorded their average thickness and the orientation of the sampled surface, which were used for shielding corrections. Separation and purification of quartz grains, as well as chemical extraction of beryllium and isotopic measurements with an accelerator mass spectrometer, were done following standard procedures at the Purdue Rare Isotope Measurement Laboratory, Purdue University. Table 2 lists the analytical sample results and the associated 1σ uncertainties, based on the propagated uncertainties in the carrier concentration, two process blanks ($^{10}Be/^{9}Be$ ratios of 5.5×10^{-15} and 3.8×10^{-15}), and the isotope measurements. We calculated exposure ages from ^{10}Be concentrations using the CRONUS-Earth online calculator v2.2 (Balco et al., 2008). The exposure ages we report here are based on the time-dependent version of the Lal (1991)/Stone (2000) production rate scaling model (Lm in Balco et al., 2008). Topographic shielding was calculated using the DEM and following Dunne et al. (1999). Shielding by snow or vegetation is negligible in the San Gabriel Mountains and was not included. Frequent wildfires in the San Gabriel Mountains could affect boulder surfaces by spallation, even if we did not see any evidence for it in the field, which would bias exposure ages to the young side. If significant, however, spallation should lead to scatter in ages from different boulders obtained from the same deposit, which, as shown here, is not significant for our study site.

RESULTS

Morphology of the Modern Valley Floor

Compared to the Bear Creek Canyon and other rivers in the San Gabriel Mountains, the modern valley floor in the North Fork San Gabriel Canyon is relatively wide and covered with alluvium, suggesting that the valley still contains substantial amounts of sediments that bury the bedrock riverbed. In fact, the only notable bedrock outcrop along the channel is at ~1 km distance from the confluence with the West Fork San Gabriel River (Fig. 2). Here, the river has cut an ~17-m-deep and ~60-m-long bedrock gorge into the eastern valley side, whereas 50 m farther west and at the same height as the gorge, terrace deposits can be seen. It thus appears that during incision of the former valley fill, the river did not reoccupy the same position within the valley but was trapped in the newly formed epigenetic gorge (e.g., Ouimet et al., 2008). The gorge is the furthest location upstream from the junction of the West Fork San Gabriel River at which we observe bedrock in the channel bed. This is in contrast to the Bear Creek Canyon, and most other rivers in the San Gabriel Mountains, which are bedrock or have only a thin veneer (<1 m) of alluvial cover (DiBiase, 2011).

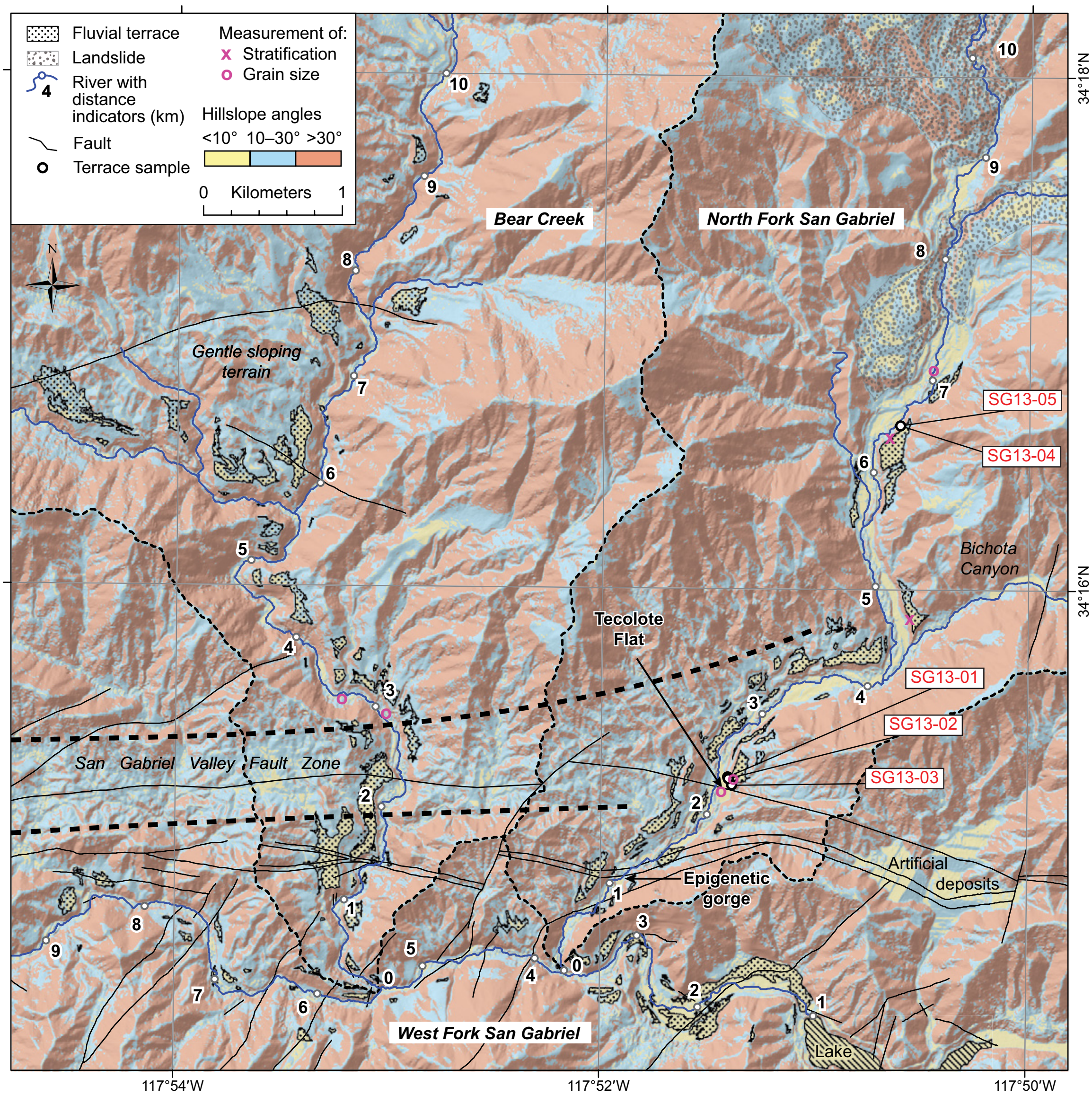

Figure 2. River terraces in the lower parts of the North Fork San Gabriel and Bear Creek Canyons. Hillshade map is color-coded by hillslope angles. Post-IR IRSL samples shown in red font.

With bankfull channel widths of 5–10 m, the active channel occupies only a small portion of the surface of the modern valley floor, which is typically 100–200 m wide. Even beyond the channel banks, the floodplain exhibits meter-scale relief, related to gullies, boulder levees, and lobate boulder deposits (Fig. 3A–D), which we infer to represent mostly debris-flow deposits (cf. Whipple and Dunne, 1992).

Longitudinal River Profiles

The longitudinal profile of a river has a characteristic shape that encodes information about its evolution and along-stream changes in the forcing and boundary conditions (Mackin, 1948; Hack, 1957). The downstream slope and upstream area of a graded river typically obey power-law scaling (e.g., Flint, 1974), and under conditions of topographic steady state, uniform lithology, climate, and rock uplift rates, the particular scaling parameters are expected to be identical across a landscape (Wobus et al., 2006; Kirby and Whipple, 2012). To analyze the scaling behavior of longitudinal river profiles and to avoid issues with DEM noise that may get exaggerated in slope data (e.g., Wobus et al., 2006), we trans-

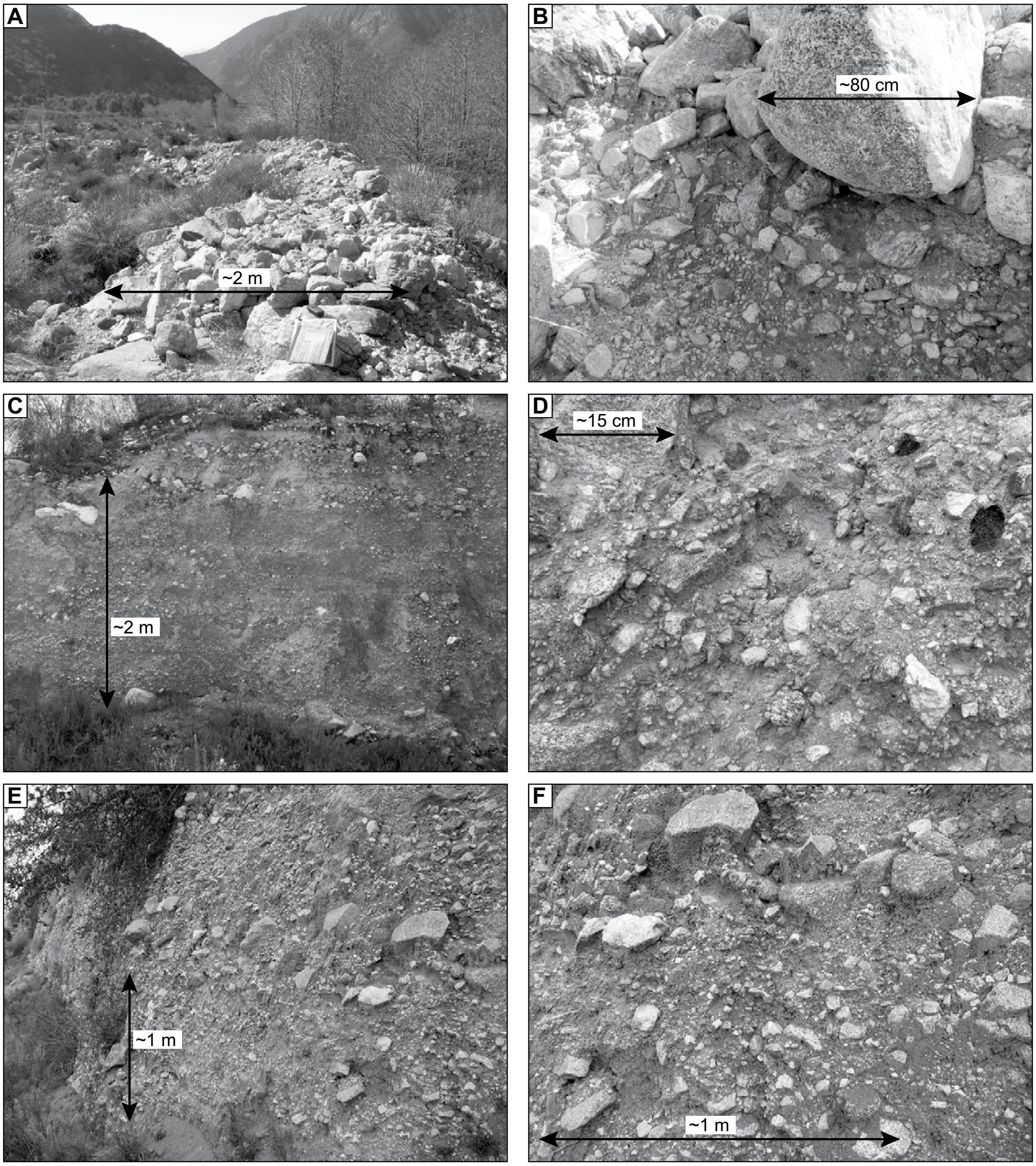

Figure 3. Field photographs of the valley floor and terrace deposits in the North Fork San Gabriel Canyon. (A) Boulder levee adjacent to the active channel (to the right, where trees grow). (B) Close-up of debris-flow channel near the debris-flow snout. (C) Exposure of poorly sorted, matrix-supported valley floor sediments near the active channel. (D) Close-up of outcrop shown in C. (E) Fill terrace (T7) at Tecolote Flat (see Fig. 2 for location), showing poor sorting but vertical variations in grain size. (F) Close-up of outcrop shown in E, with subangular clasts in fine-grained matrix, similar to modern valley floor outcrop in D.

formed the horizontal coordinate (distance) of channel elevation data by upstream integration, and minimized the misfit between the resulting so-called χ plot and a straight line (Perron and Royden, 2012).

Analysis of the North Fork San Gabriel River and Bear Creek channels shows that the degree to which the slope-area data obey power-law scaling differs between the two drainage networks (Fig. 4). In particular, the North Fork San Gabriel shows considerably greater deviations of the individual profiles from a straight line than the Bear Creek profile. Furthermore, the largest tributary of the North Fork San Gabriel River displays more gentle slopes than the main-stem river, resulting in lower elevations at similar distance from their confluence. It should be noted, however, that this tributary (Bichota Canyon) appears to follow a branch of the San Gabriel fault, which may partly explain the unusual morphology. Quite different from this, the channel maintains a relatively constant gradient across the epigenetic gorge and does not have a pronounced knickpoint (Fig. 4), despite the strong lithological contrast between the bedrock and the valley fill, and the abundance of waterfalls elsewhere in the San Gabriel Mountains (DiBiase et al., 2015). Nevertheless, the peculiar profile of the North Fork San Gabriel River in its upper reaches coincides with the extent of landslide deposits, suggesting that this part of the drainage is not in topographic equilibrium. In contrast, the longitudinal profile of the Bear Creek appears relatively graded for most of its length, and the main stem and its tributaries share rather similar channel steepness values, although deviations from a graded profile exist. These could be related to transient adjustments to changes in tectonic forcing (e.g., DiBiase et al., 2015).

Spatial Distribution of Terraces

River terraces in the North Fork San Gabriel Canyon are exclusively found along the lower 7 km of the valley and range in character and size from possible terrace remnants a few meters wide and long, to well-developed flat terrace treads of up to ~70,000 m^2 in area (Fig. 2). In the lower 4 km of the valley, we identified at least six different terrace levels, with heights ranging between ~2–5 m and ~85 m above river level (arl; Fig. 5A). The most extensive level, at ~40 m arl, corresponds to Bull's (1991) T7 terrace. Lower terraces appear to be cut into the T7 valley fill. Higher terraces are less frequent and more difficult to identify and to trace along the valley. At a distance of 4–5 km from the outlet, where the North Fork San Gabriel River turns northward, the T7 terrace surface decreases in elevation and eventually disappears farther upstream. The highest upstream-located, well-developed terrace surface is at ~20 m above the river bottom. Because of the similarity in extent, this terrace may represent the continuation of T7, as already noted by Bull (1991), which would require a significant decrease in height above the river. The T7 and younger terraces are clearly fill terraces, as shown at several outcrops where the entire stratigraphy, from the modern valley floor to the top terrace surface, is exposed. For the higher (older) terraces (T4 and T1 in Bull, 1991), this cannot be ascertained due to the lack of exposure.

It is notable that the majority of terraces are located on the northwestern bank of the North Fork San Gabriel River, and that they are most abundant between ~1 and 5 km distance from the confluence with the West Fork of the San Gabriel River. This valley reach coincides with a zone of subdued relief (Fig. 2) that traces the San Gabriel fault zone across the Bear Creek Canyon before branching off the main fault zone in a northeastern direction to follow a fault branch along the North Fork San Gabriel and Bichota Canyons (Jennings and Bryant, 2010). Surprisingly, however, we found no terraces in Bichota Canyon.

River terraces are also abundant in the Bear Creek Canyon, and they are predominantly found in the lower ~8–9 km of the valley (Fig. 2). In contrast to the North Fork San Gabriel Canyon, all terraces that we observed in Bear Creek Canyon were strath terraces, with fluvial gravels of a few meters thickness, at most, resting on top of bedrock. Unlike terraces in the North Fork San Gabriel Canyon, terraces in the Bear Creek Canyon have similar heights and define at least two pronounced terrace levels at ~35 m and ~77 m arl (Fig. 5B). The higher level is more abundant in the upper reaches of the Bear Creek Canyon, and, in many places, the terrace surfaces can be seen to transition into gentle-sloping colluvial hillslopes (Fig. 2). Other terrace levels are less well expressed or indistinguishable from the two more pronounced levels.

River terraces also exist along the West Fork San Gabriel River, but their distribution is more restricted (Fig. 2). Since its construction in 1939, the San Gabriel Dam, which is located ~3.5 km downstream from the confluence of the East and West Forks of the San Gabriel River, has forced the river to aggrade its bed, as far as 3 km upstream from the confluence. Beyond this distance, the only terraces we observed are strath terraces of relatively small extent (~50 m × 50 m). We extrapolated the two most pronounced terrace surfaces in the Bear Creek and North Fork San Gabriel Canyons into the West Fork, to examine whether they line up with other distinct terrace levels (Fig. 5C), although we acknowledge that correlating terraces across watersheds by elevation can be problematic. The lower terrace level in Bear Creek Canyon (~35 m arl) is very close

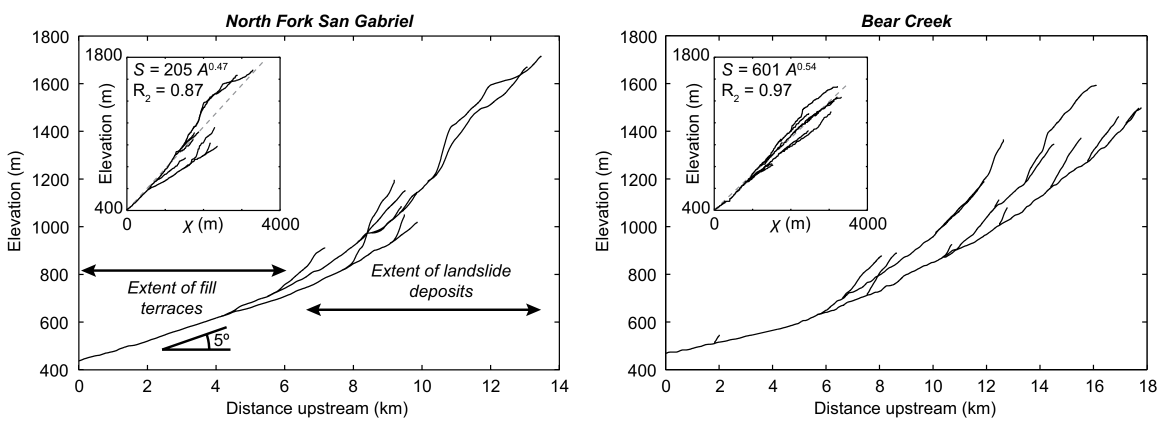

Figure 4. Longitudinal profiles of the North Fork San Gabriel and Bear Creek drainage networks. Inset figures show best fitting χ-transformed drainage networks and the resulting slope-area scaling. See text for details.

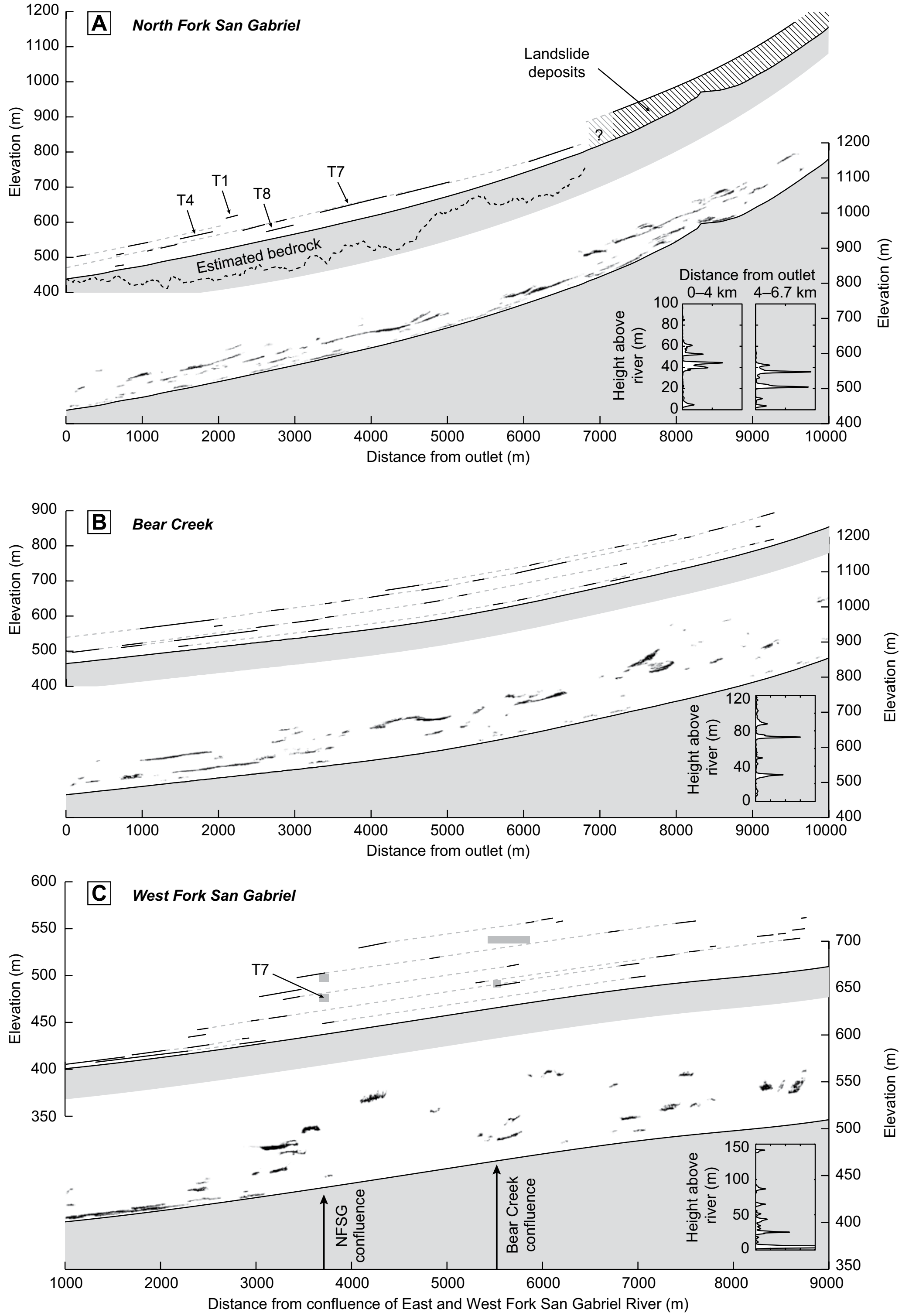

Figure 5. Terrace surface elevations along (A) the North Fork San Gabriel River (NFSG), (B) Bear Creek, and (C) the West Fork of the San Gabriel River. In each panel, the lower part shows terrace surfaces that have been projected into a plane following the rivers. The upper part shows the corresponding interpretation of correlated terrace treads. Inset to lower right shows smoothed histogram (0.1 m bins) of terrace surface heights above present-day rivers. Gray rectangles in C denote the expected position of terrace surfaces joining from the North Fork San Gabriel and Bear Creek Canyons. Estimated bedrock elevation in A is derived from reconstruction shown in Figure 7B. See text for details.

($\Delta z < 5$ m) to two terrace levels in the West Fork. For the upper terrace level (~70 m arl), the exact position of the confluence with the West Fork is not well constrained, but it appears poorly aligned with higher terrace levels in the West Fork Canyon. The two most pronounced terrace levels in the North Fork San Gabriel Canyon align only partly with corresponding terrace levels in the West Fork. Whereas the T5 terrace level in the North Fork San Gabriel Canyon might be related to the upper terrace level in the Bear Creek Canyon, the widely distributed T7 terrace level appears to be distinctly different from any terrace surfaces in the Bear Creek Canyon.

Terrace versus River Gradients

Present-day river gradients in the North Fork San Gabriel Canyon cluster around 0.05 and 0.08, corresponding to reaches below and above the junction with Bichota Canyon, respectively (Fig. 6). Terrace surface gradients along the

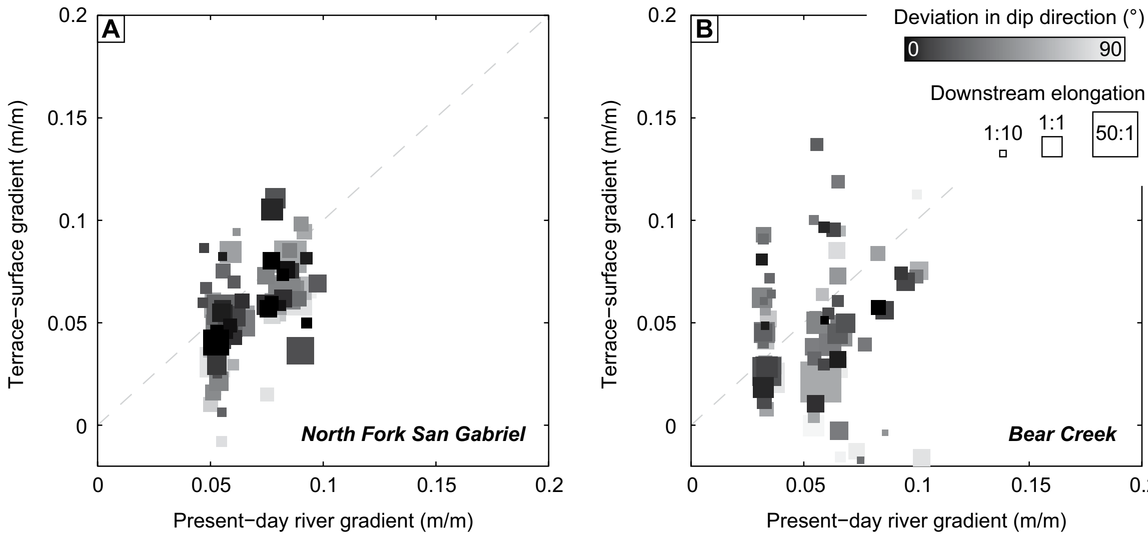

Figure 6. Comparison of downstream gradients of present-day river and terrace surfaces (A) in the North Fork San Gabriel Canyon between 0 and 6.7 km upstream distance from the outlet, and (B) in the Bear Creek Canyon between 0 and 10 km upstream distance from the outlet. Size and color coding of the marker symbols are the same in both panels. Downstream elongation is defined as the ratio of the downstream and the across-stream extent.

channel axis direction occupy a wider range of values, ~0–0.1, and are on average slightly less steep than the active channel. River gradients in Bear Creek Canyon are typically lower, between 0.03 and 0.06, although upstream parts of the river steepen to 0.1. Terrace gradients in Bear Creek occupy a similar range as those in the North Fork San Gabriel, but they appear on average somewhat gentler than the corresponding river gradients. In both canyons, the shallowest gradients are typically associated with terrace surfaces for which the true dip is highly oblique to the valley axis, and which have a rather small downstream elongation; that is, their across-valley extent is large relative to their down-valley extent. These attributes indicate that the measured surface gradients are associated with relatively higher uncertainties.

Valley Fill Reconstruction

Based on the spatial distribution of T7 terrace surfaces in the North Fork San Gabriel Canyon, we estimated the elevation of the corresponding former valley fill surface (Fig. 5A). After projecting terrace pixels into the flow path, we sought a visual fit of all T7 terraces with piecewise splines. The along-valley distance of each terrace pixel was obtained by creating a 1-km-wide swath that followed the valley using functions from the TopoToolbox v2 (Schwanghart and Scherler, 2014). The resulting one-dimensional valley fill surface was extended laterally by assuming across-valley constant heights, again using the 1-km-wide swath. Finally, each pixel was assigned the maximum value of the valley fill surface and the modern topography (cf. Scherler et al., 2015). Subtracting the present-day topography from the valley fill surface yields an estimated volume of ~0.034 km^3 of material that has been eroded since abandonment of the T7 surface (Fig. 7A). We also estimated the bedrock elevation beneath the valley fill, by projecting the adjacent hillslopes at an angle of 35° into the subsurface. This hillslope angle is representative for bedrock hillslopes in the North Fork San Gabriel and Bear Creek Canyons (Fig. 2; DiBiase et al., 2010). Although this approach is rather crude and misses details of the true bedrock surface, it allows us to obtain a rough estimate of the volume of material that is still stored in the valley. By subtracting the estimated bedrock elevation from the reconstructed T7 surface, we estimate the total volume of the valley fill to be of the order ~0.1 km^3 (Fig. 7B). The estimated depth to bedrock increases with upstream distance from the outlet of the North Fork San Gabriel and reaches its maximum depth of >100 m below the present-day valley bottom near the junction with the Bichota Canyon. Farther upstream, valley narrowing results in a decrease of the estimated depth to bedrock to <50 m, followed by another increase toward the transition from the terraces to the landslide deposits.

Terrace Stratigraphy

At small spatial scales (centimeters), the sediments exposed at terrace outcrops do not show any stratification (Figs. 3E and 3F). At larger spa-

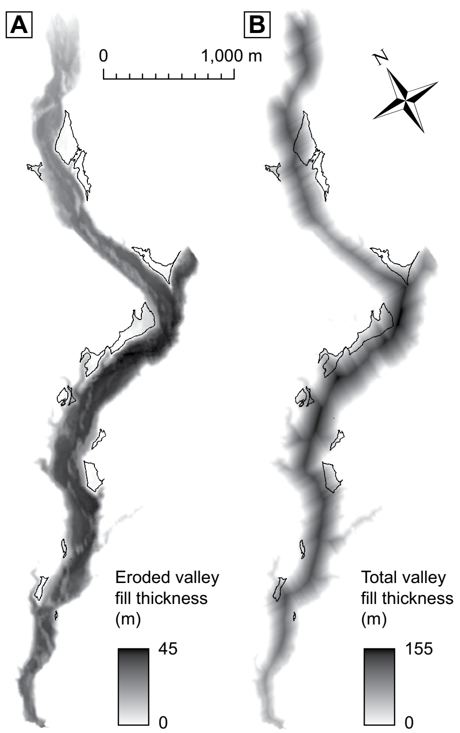

Figure 7. Estimated valley fill thickness in the North Fork San Gabriel Canyon. (A) The eroded valley fill thickness corresponds to the elevation difference between the reconstructed T7 terrace level and the present-day topography. (B) The total valley fill thickness is the elevation difference between the reconstructed T7 terrace level and the reconstructed bedrock at the base of the valley fill. Black lines delineate T7 terrace surfaces.

tial scales, coarse-grained, poorly sorted lenses of subrounded to subangular boulders and cobbles that are roughly ~0.5–2 m thick and 20 m wide are vertically separated by ~2 m from finer-grained matrix-supported deposits (Fig. 8B). The transition between the coarse-grained lenses and the fine-grained deposits is gradual and not well defined. These assemblages look similar to the levee-snout topography on the modern floodplain. At two locations along the North Fork San Gabriel River, we measured the dip of the coarse-grained lenses from outcrops that parallel the valley trend using a laser range finder (Fig. 2). Near the upstream end of the terraces, at 6.3 km distance from the outlet, these lenses dip at 0.11–0.12 (n = 2), which is slightly steeper than the gradient of the river (~0.1) and of the terrace surface (~0.07). At a distance of 4.7 km from the outlet, the lenses dip at ~0.05–0.06 (n = 3), which in this case is less than the gradient of the river (~0.08) and of the terrace surface (~0.08).

Fluvial response to climate change is expected to produce grain-size variations (Armitage et al., 2011). The grain size of the sediment within the terraces, however, is not markedly different from that of sediment in the modern channel and on the floodplain, or from sediment on the floodplain of Bear Creek (Fig. 9). Median grain sizes (D_{50}) of the terrace deposits range between 22 and 60 mm in diameter (Table 3). Although our grain-size measurements from the active channel and floodplain of the modern valley floor indicate on average coarser grains compared to the terraces, this difference may simply be due to the effect of sorting, in which both debris-flow deposits and riverbeds tend to have coarser grains near their tops (e.g., Parker and Klingeman, 1982; Takahashi, 2014). Significant variability in grain sizes was also observed by DiBiase and Whipple (2011) in a study covering the entire San Gabriel Mountains, where median grain sizes (D_{50}) ranged between ~22 and 180 mm. From Figure 8B, it is clear that significant grain-size variations exist within individual terrace deposits—a fact that is also reflected in the different grain-size distributions that we and Bull (1991) obtained from the same T3 deposit (Fig. 9). Finally, it is notable that we observed by far the largest grain sizes in our survey of the active channel immediately downstream of the landslide deposits. Bull (1991) reported similar values from an active channel (SC), but the location was not documented.

Post-IR IRSL Depositional Ages

The three available ^{14}C ages that were obtained by Bull (1991) stem from a 40-m-high and ~150-m-wide terrace outcrop at Tecolote Flat (Fig. 2). This is a key locality where the hypothesis of multiple cut-and-fill events can be tested, because the outcrop exposes gravels

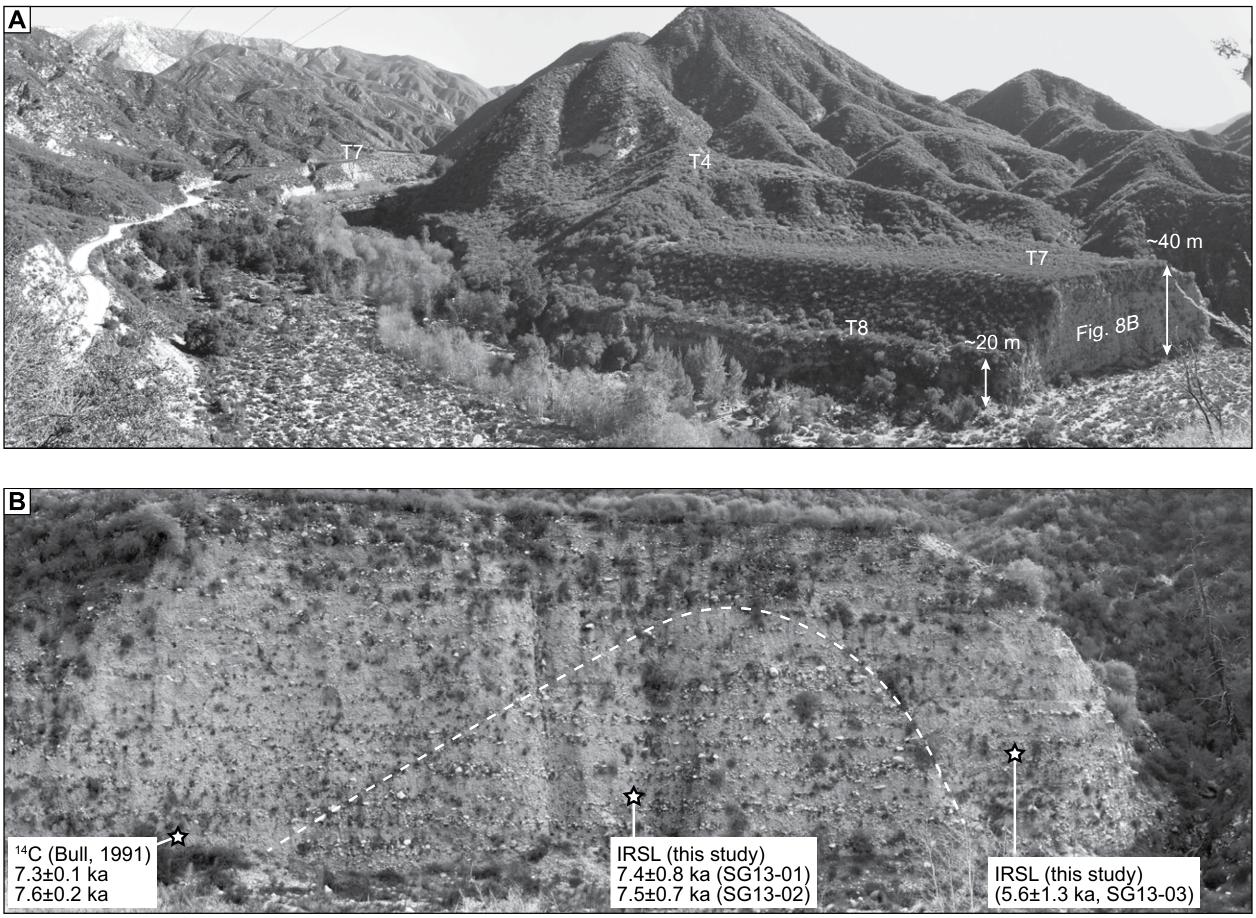

Figure 8. River terraces in the North Fork San Gabriel Canyon. (A) View upstream from road near Tecolote Flat. T4, T7, and T8 denote terrace levels originally defined by Bull (1991). The river is concealed by bare-branched trees. (B) Fill terrace outcrop (40 m high) at Tecolote Flat. Dashed white line marks boundary that was proposed by Bull (1991), between a stratigraphically older (T3) and younger valley fill (T7). See the supplementary material for a color version of the photograph in Figure 8B (see text footnote 1). Ages in B are from Bull (1991) and infrared stimulated luminescence (IRSL; this study).

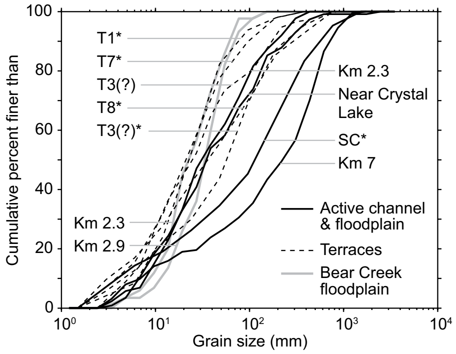

Figure 9. Grain-size distributions for modern river and terrace sediments. Question marks behind "T3" indicate uncertainty whether this deposit is truly different from T7. See text for details.

TABLE 3. GRAIN-SIZE COUNTING RESULTS

Location	Number of measurements n	Grain size (mm) D_{16}	D_{50}	D_{84}
North Fork San Gabriel Canyon				
Near Crystal Lake (channel)	123	9	35	150
Km 7 (channel)	191	11	215	586
Km 2.3 (floodplain)	100	10	31	128
Km 2.3 (terrace T3)	137	4	20	121
SC* (channel)	97	8	120	406
T1* (terrace)	99	9	23	55
T3* (terrace)	98	8	60	174
T7* (terrace)	100	6	22	73
T8* (terrace)	97	6	38	183
Bear Creek				
Km 3.3 (floodplain)	111	15	34	59
Km 2.9 (floodplain)	117	12	23	52

*Based on grain-size histograms given in Bull (1991).

that are associated to the T7 terrace, and according to Bull (1991), presumably also older (T3) deposits that were buried by the T7 gravels and are now reexposed. Due to the poor sorting of the sediments, we found it difficult to pin down the contact between these units at the outcrop, whereas at greater distance, differences in grain size and color are apparent (Bull, 1991; see Fig. S1 in the supplementary material). In the lower-left part of Figure 8B, the dashed line follows a ledge in the modern face of the cliff that is decorated with vegetation (cf. Fig. S1 [see footnote 1]), and it raises the impression that the T3 deposit is actually adjoining the T7 deposit laterally and therefore younger.

To shed light on the stratigraphic order of these deposits, we collected three IRSL samples at Tecolote Flat. The first two (SG13-01 and SG13-02) stem from the apparent T3 deposit, close to the base of the terrace (Fig. 8B), and are vertically separated by only ~1 m. With depositional ages of 7.4 ± 0.8 ka (SG13-01) and 7.5 ± 0.7 ka (SG13-02; Fig. 10), both samples yielded ages that are statistically indistinguishable from Bull's (1991) ^{14}C ages of 7.3 ± 0.1 ka and 7.6 ± 0.2 ka, which came from the T7 deposit to the left of the T3 deposit. Our third sample (SG13-03) was collected from the T7 deposit at a stratigraphically higher, and hence younger, position, compared to Bull's (1991) ^{14}C samples and is located to the right of the T3 deposit. This sample displays very poor bleaching, with only a single result representing a well-separated minimum age peak at 5.6 ± 1.3 ka (SG13-03; Fig. 10). This single result is from 116 grains that provided finite age results of 400 measured in total for this sample. Note that given the significant 1σ uncertainty, this sample may be consistent in depositional age with the two lower samples from this exposure, or it may have been deposited somewhat later. Because the population of old grains is very similar to the samples SG13-01 and SG13-02, we think that this sample is just very poorly bleached, due to insufficient exposure to sunlight. Therefore, our new IRSL ages agree with the available ^{14}C ages by Bull, and they do not support an old (T3) valley fill covered by the T7 terrace. An alternative explanation is that the T3 deposit truly adjoins the T7 deposit laterally but has been eroded in its central part, exposing the T7 material that we dated. However, this scenario appears unlikely because coarse-grained layers can be traced continuously across the face of the presumable T3 deposit. More samples and observations are needed to unravel the stratigraphic context of these units.

The other two samples were taken from a terrace outcrop near the uppermost limit of the fill terraces, close to the first occurrence of landslide

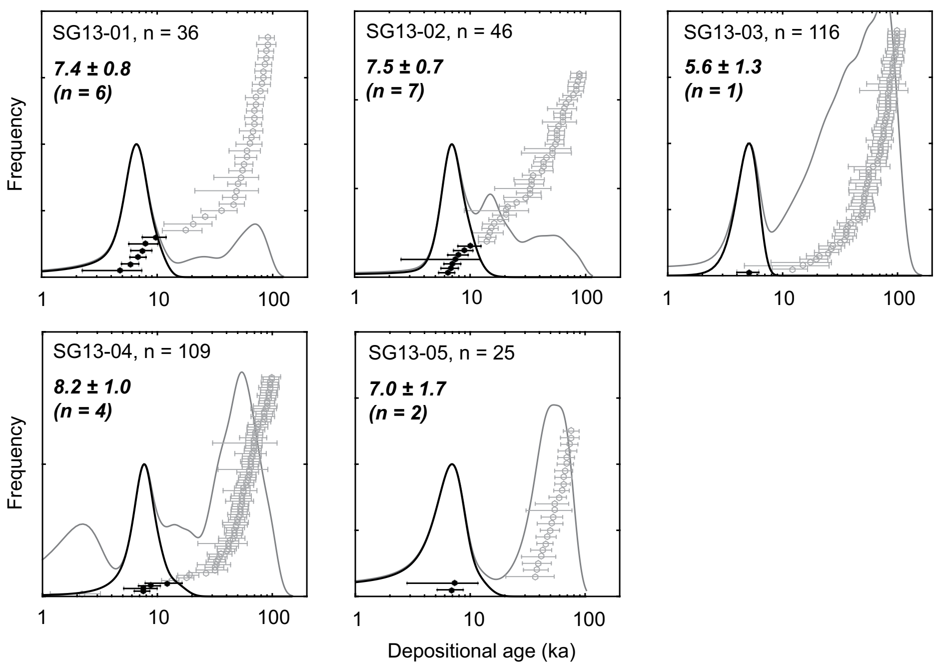

Figure 10. Apparent age and probability density functions of single-grain Postinfrared infrared stimulated luminescence (IRSL) determinations (all results in gray; grains selected for age estimation in black). The text inside the axes provides the sample ID and the number of grains that produced a finite age estimate (top row), the depositional age with 1σ uncertainties obtained from selected grains highlighted in black (middle row), and the number of grains contributing to the age (bottom row). The samples are dominated by a broad distribution of many unbleached or poorly bleached grains, and a young age peak. See text for details.

deposits (Fig. 2). These samples yielded again very few grains that we considered potentially bleached. The most likely age of SG13-04 is 8.2 ± 1.0 ka, based on only four grains. We discarded one grain that gave an even younger age of ca. 2 ± 1 ka, which we think might have been related to a bird burrow that we encountered at the sampling site. The stratigraphically higher, and hence younger, sample SG13-05 gave an age of 7.0 ± 1.7 ka, based on only two grains. Again, the population of old grains in these two samples is very similar to that of the other samples, which we interpret to be the result of incomplete bleaching.

Landslide Deposits

Crystal Lake Landslide

Based on their morphology and distribution, we distinguished at least three different landslide deposits in the upper North Fork San Gabriel Canyon (Fig. 11). The most extensive deposit belongs to the Crystal Lake (CL) landslide and covers an area of ~7 km^2, situated between ~1000 and ~2000 m elevation. Approximately half of the area lies at an elevation above 1600 m and constitutes a broad, pan-shaped alluvial surface, which is surrounded by bedrock hillslopes that transition into scree slopes, debris-flow channels, and debris fans. Several smaller intermittent creeks occupy this surface and leave it in its southeastern corner, where they merge to form Soldier Creek. Large parts of this upper level appear to constitute reworked landslide deposits and active fluvial and debris-flow depositional areas, which prevented us from collecting any samples there. Crystal Lake itself is confined to a small topographic depression in the southwestern corner of the upper level, adjacent to steep bedrock hillslopes in the west and an elongated, north-to-south–trending topographic ridge in the east. This so-called Sunset Ridge can be traced for >3 km as a distinct morphological feature that is associated with large and angular, gneissic-granitic boulders on its surface. Although no clear detachment scars can be seen in the field, Sunset Ridge, and the morphology of the surrounding hillslopes, suggests that the source areas of the Crystal Lake landslide were located to the north and east of this upper level (Morton et al., 1989). Below the upper low-relief area, there is another, less-extensive one, which is located at elevations of around 1400 m. These two levels are separated by a topographic step, which features an ~500-m-wide slump along its steepest part. West of the lower level, additional gentle-sloping surfaces are located ~150–200 m higher, but farther to the south, they join into the same level. Below ~1350 m, the Crystal Lake

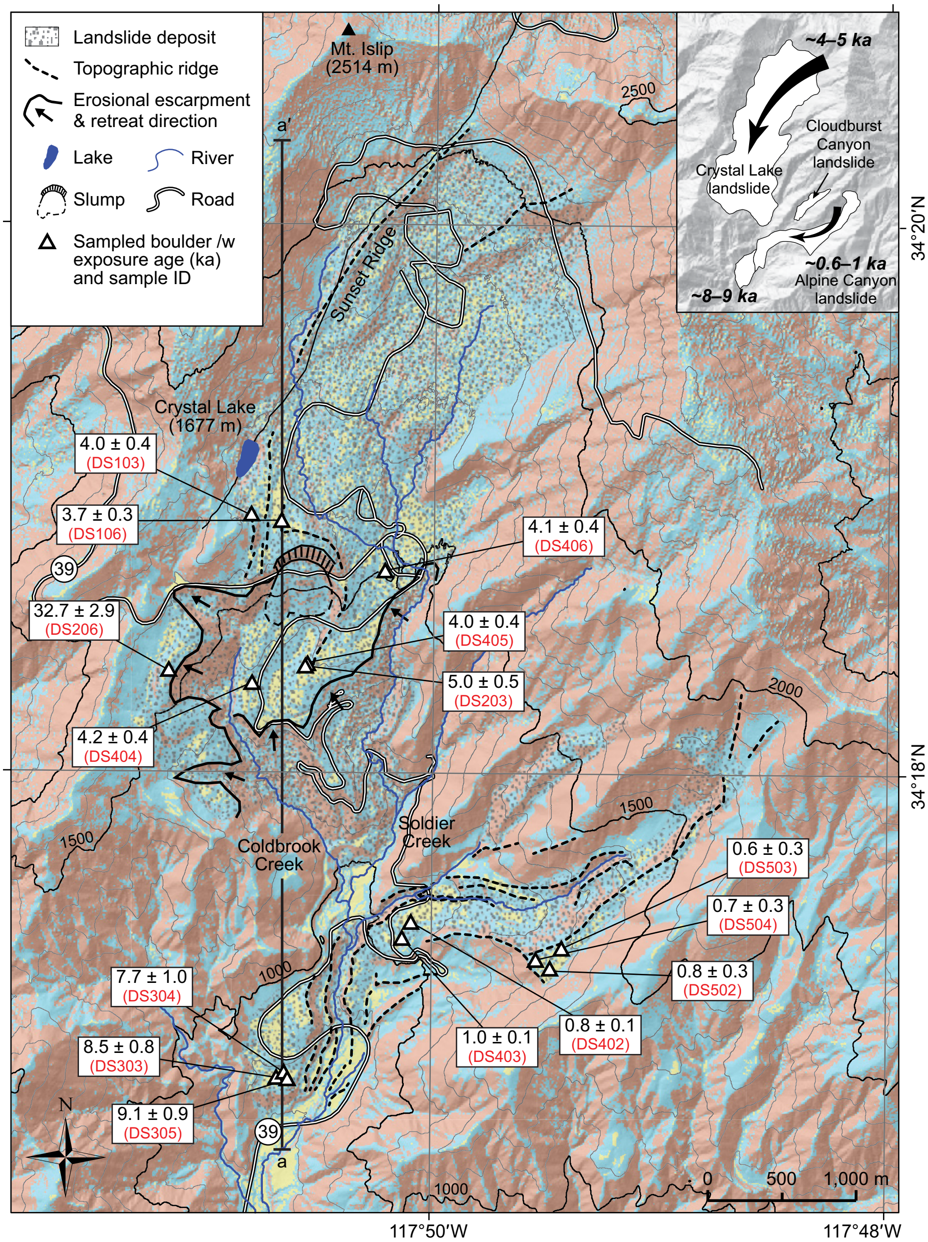

Figure 11. Map of landslide deposits in the headwaters of the North Fork San Gabriel Canyon. Upper-right inset shows tentative chronology of landslide events, constrained by ^{10}Be-surface exposure ages. Topographic profile a-a′ is shown in Figure 16.

landslide deposit is exposed on steep hillslopes and confined on either side by Coldbrook and Soldier Creeks, which are actively incising headward, thereby creating pronounced erosional escarpments.

We collected seven samples from boulders that we associate to the Crystal Lake landslide for surface-exposure dating with ^{10}Be. Three of the samples (DS103, DS106, and DS406) stem from boulders situated on the upper level, but at opposing sides of the valley. All three samples yielded ages that overlap within uncertainties (Fig. 11; Table 2), with an average age of ca. 3.9 ± 0.2 ka. Three more samples (DS203, DS404, and DS405) that we collected from boulders on the lower low-relief area yielded similar ages, with an average age of ca. 4.4 ± 0.25 ka. The slightly older age is due to sample DS203, which gave an age of ca. 5.0 ± 0.5 ka, which in turn may be due to inheritance, as an adjacent boulder yielded an age of 4.0 ± 0.4 ka (DS405). Our last sample (DS206) from the Crystal Lake landslide stems from the gentle-sloping area that is located west of and ~150 m above the lower three samples. This boulder has an exposure age of ca. 33 ± 3 ka. As this is our only sample from the Crystal Lake landslide with an age markedly older than mid-Holocene, it is difficult to provide a concluding explanation. Because the boulder rests on relatively low-sloping terrain that is at a markedly higher elevation than the areas farther to the east, it may be that these surfaces represent remnants of an older deposit.

Alpine Canyon Landslide

The Coldbrook and Soldier Creeks join at the toe of the Crystal Lake landslide and flow for another ~500 m across a gentle-sloping alluvial reach before they dissect the lower part of the Alpine Canyon landslide. The Alpine Canyon landslide covers an area of ~1.3 km^2, between ~900 and ~1800 m elevation, and it is steeper and narrower than the Crystal Lake landslide. The canyon's drainage originates at ~2300 m, near the highest point of the catchment, and it is first manifested as a debris-flow channel with a slope of ~0.62 that has been carved ~50 m into the bedrock (Fig. 12). Near ~1700 m, the channel encounters the landslide deposit, marked by a pronounced topographic step (Fig. 12B). Between an elevation of ~1500 and 1300 m, the channel has a slope of ~0.23 and is paralleled by an ~2-km-long topographic ridge that straddles the southeastern valley side. This ridge is quite similar to the Sunset Ridge at the Crystal Lake landslide, although it is less vegetated and bounded by a steep slope at the valley side. The area between the ridge and the hillside occupies a subhorizontal, hummocky surface that is mantled by coarse and angular boulders (Fig. 13B). This boulder field extends for more than 1 km, parallel to the canyon, and terminates at an east-west–striking interfluve, suggesting that landslide material overtopped the barrier to the south. Along the lower 3 km, the Alpine Canyon landslide has an average surface gradient of ~0.13 and develops a slightly convex surface that has been dissected by the intermittent Alpine Canyon Creek. Between the transverse profiles "e" and "f" in Figure 12, the so-called Cloudburst Canyon is cut ~35 m into the landslide surface (Fig. 14) and bounded by hillslopes with slope angles of 40° and more.

We collected five samples from boulders that we associate with the Alpine Canyon landslide. Three of the samples (DS502–DS504) stem from the boulder field in the southeastern corner of the landslide, at an elevation of ~1250 m (Fig. 13B). The three ages overlap within uncertainties and yield an average age of 0.7 ± 0.2 ka. The other two samples (DS402–DS403) stem from boulders from the surface of the main landslide deposit near Cloudburst Canyon and have similar ages of ca. 0.9 ± 0.1 ka. For a maximum landslide age of ~1000 yr, the 35 m of incision at Cloudburst Canyon yields a time-averaged incision rate of 35 mm yr^{-1}.

The lowermost landslide deposit is found near the toe of the Alpine Canyon landslide, which led Morton et al. (1989) to suggest that it is part of

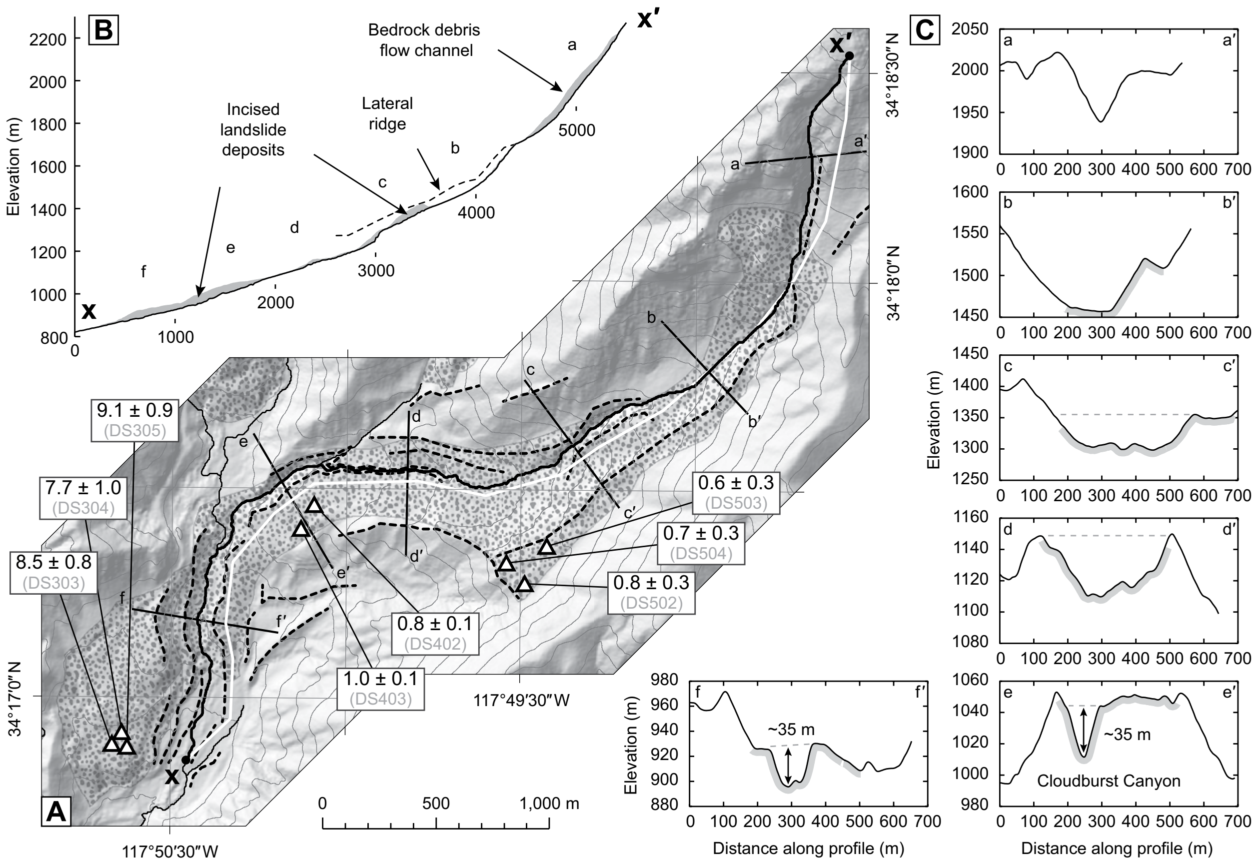

Figure 12. Morphology of the Alpine Creek landslide. (A) Hillshade map showing landslide deposits (dotted), topographic ridges (dashed black lines), and trace of topographic profiles (solid black lines). Triangles indicate dated boulders. Contour interval is 50 m. (B) Longitudinal profile along channel marked x-x′ in A. Gray areas denote incision of channel into bedrock and landslide deposits, as obtained from white profile next to the channel in A. Positions of transverse profiles shown in C are marked by lowercase letters (a–f). (C) Topographic profiles transverse to the downvalley direction. Thick gray lines mark distribution of landslide deposits.

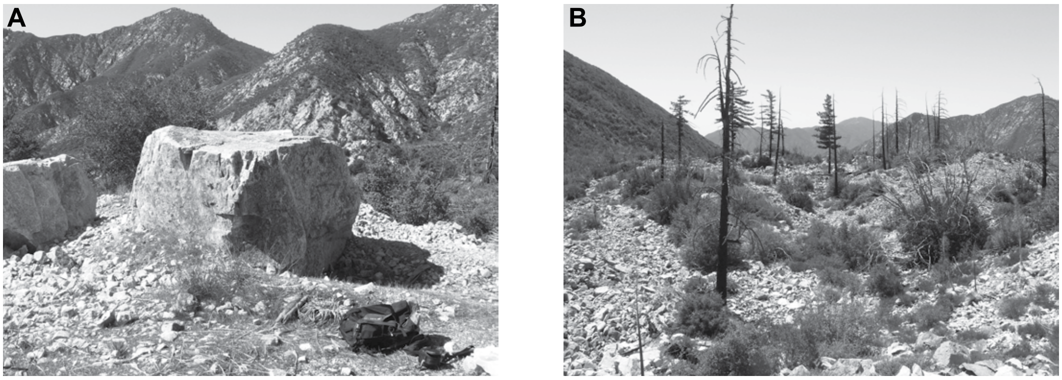

Figure 13. Landslide boulders. (A) Typical granitic-gneissic boulder that was sampled for surface exposure dating (DS403). Boulder height is ~1.5 m. (B) Boulder field atop topographic ridge associated with the Alpine Canyon landslide, near sample DS503. View is to the southwest. Field of view in the center of the photograph is ~150 m.

the same landslide. However, the deposit, which has an area of ~0.4 km^2 and an average elevation of ~950 m, is ~50 m higher than the adjacent surface of the Alpine Canyon landslide, precluding a common origin. Similar to the terminal part of the Alpine Canyon landslide, the river-facing slope forms a steep (>30°) erosional escarpment and a gentle-sloping surface that dips away from the river toward the western hillslopes, somewhat resembling the morphology of a large levee. Much of the northern half of this deposit has undergone surface modification by human activity, deposition in closed depressions, or colluvial deposition from adjacent hillslopes. Three samples (DS303–DS305) that we collected from boulders near the southern limit of the deposit have exposure ages that overlap within uncertainties and yield an average age of 8.4 ± 0.5 ka.

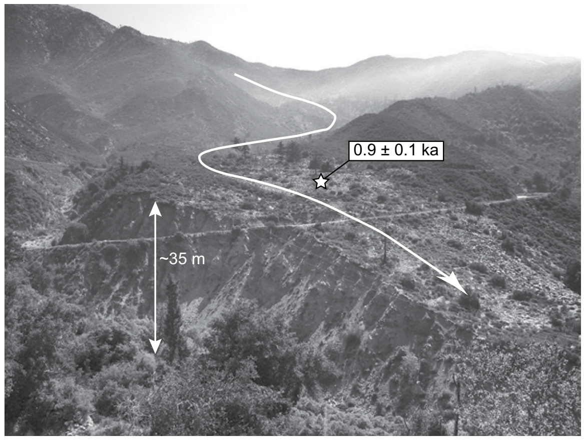

Figure 14. Field photograph of the Alpine Canyon landslide and Cloudburst Canyon. The landslide surface has been dissected by ~35 m. Star indicates sampled boulders with an exposure age of ca. 0.9 ± 0.1 ka.

Summary Landslide Deposits

Our exposure ages from boulders on the landslide deposits define three age populations (Fig. 15). The oldest population yields an age of ca. 8–9 ka and refers to the lowermost landslide deposit. Given our simplifying assumption of negligible erosion of the boulder surfaces, this is likely a minimum age. Because this deposit is unrelated to the adjacent, but topographically lower, ca. 0.5–1 ka Alpine Canyon landslide deposit, we suggest that it represents a remnant of the initial Crystal Lake landslide, which would have extended farther downstream than it does today. Gentle-sloping hillslopes at ~1500 m elevation, west of the Coldbrook Creek (Fig. 11), could indicate a formerly continuous surface that connected the upper level of the Crystal Lake landslide with the lowermost deposit (Fig. 16). We interpret the ca. 4–5 ka boulders on the upper part of the Crystal Lake landslide as representing another landslide event that could have occurred either independently (cf. Morton et al., 1989), or as a secondary failure within the deposits of the initial landslide. Fresh landslide deposits typically display hummocky topography where surface waters can accumulate in local depres-

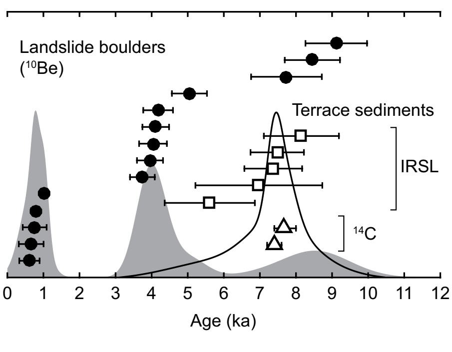

Figure 15. Sample ages and combined probability density function for landslide boulders (solid) and terrace sediments (hollow) in the North Fork San Gabriel Canyon. Postinfrared infrared stimulated luminescence (post-IR IRSL; squares) and ^{10}Be ages (circles) are from this study; ^{14}C ages (triangles) are from Bull (1991). Error bars reflect 1σ (IRSL, ^{14}C) and external uncertainties (^{10}Be; cf. Balco et al., 2008).

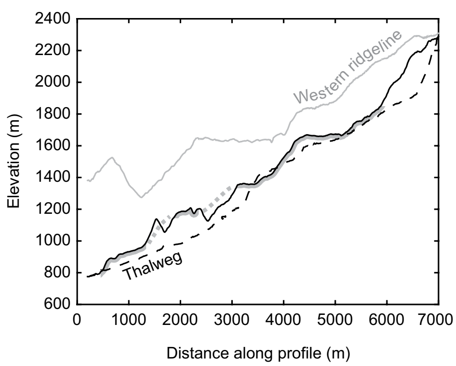

Figure 16. Topographic profile across the Crystal Lake landslide. Solid black line gives elevation along profile a-a′ shown in Figure 11. Bold gray line indicates landslide deposits, broken where inferred. Thalweg and ridgeline elevations are projected into the profile.

sions and facilitate secondary slope failures by exerting hydrostatic pressure on the surrounding materials. The slump that borders the higher part of the Crystal Lake landslide could represent such a process at small spatial scale.

DISCUSSION

Our results bring new data to bear on deep-seated landsliding, fill terraces, and a potential connection between the two in the North Fork San Gabriel Canyon. First, we evaluate the hypothesis of Bull (1991) that the fill terraces are a result of climate-change–induced changes in sediment supply. Second, we discuss our preferred interpretation that the fill terraces are a result of increased sediment supply and debris-flow activity following deep-seated landslides. Third, we discuss the timing of deep-seated landsliding and potential triggers. Fourth, we discuss the implications of our findings for landscape evolution in the San Gabriel Mountains and for the ways in which rapidly eroding landscapes respond to climate change.

Fill Terrace Formation Caused by Climate Change?

Bull (1991) argued that valley aggradation in the North Fork San Gabriel Canyon (and elsewhere in the San Gabriel Mountains) was due to climatic changes that caused an increase of hillslope sediment supply relative to the transport capacity of rivers. Although Bull (1991) essentially applied the climate change model to all terraces in the North Fork San Gabriel, he focused on the T7 terrace, which is also the focus in our study. In this model, the principal mechanism of valley aggradation is fluvial deposition of bed load, which we find difficult to reconcile with our observations. First, there is no record of a major climate shift over the last 7 k.y. Instead, reports of paleoclimatic conditions in Southern California during the early Holocene are diverse. For example, Owen et al. (2003) and Kirby et al. (2007) found indications that the early Holocene may have been a time of higher rainfall than today, whereas periods of dune activity and paleolakes in the Mojave Desert suggest that the entire Holocene was comparatively drier than the latest Pleistocene, including the Last Glacial Maximum (Tchakerian and Lancaster, 2002). Furthermore, the Holocene aggradation episode in the North Fork San Gabriel Canyon was concurrent with a period of downcutting from ca. 10 to 2 ka in the Cajon Creek area that followed extensive aggradation between 16 and 10 ka (Weldon and Sieh, 1985). Studies from other places around the western Transverse Ranges indicate that one or several major pulses of aggradation and alluvial-fan formation occurred between ca. 60 and 30 ka (Weldon and Sieh, 1985; Matmon et al., 2005; Van der Woerd et al., 2006; Fletcher et al., 2010; Behr et al., 2010; McGill et al., 2013; Owen et al., 2014).

Second, the spatial confinement of fill terraces to the North Fork San Gabriel Canyon is at odds with climatic forcing and gradual deposition by rivers, which ought to have had a more regional impact on the drainage network. One explanation could be that the rate of incision into the valley fill had been limited by the epigenetic gorge in the lower part of the North Fork San Gabriel Canyon (Fig. 2) and thereby allowed preservation of much of the valley fill, which was more rapidly eroded in neighboring canyons like that of Bear Creek. This scenario, however, does not explain why fill terraces are absent from the Bichota Canyon because it is a tributary to the North Fork San Gabriel Canyon and should have responded in a similar way. This suggests an evenly distributed valley fill has never existed to the same extent as in the North Fork San Gabriel Canyon, perhaps because very rapid deposition and incision of the valley fill in the North Fork San Gabriel Canyon prevented significant backfilling.

Third, the materials that make up the terrace deposits do not have a clear fluvial signature. The lack of sorting, the mostly subangular clasts without any discernible imbrication, a matrix-supported texture, the lack of fine-scale lamination, and the high amount of sandy to granular matrix material are more typical of debris-flow deposits. The high slopes (0.05–0.1) of the present-day river channel, the terrace surfaces, and the stratification within the valley fill are indeed consistent with slopes reported from debris-flow channels (Stock and Dietrich, 2003) and support our observations of debris-flow levees and snouts (e.g., Whipple and Dunne, 1992) across the modern valley floor. Furthermore, the dominance of grains in our terrace sediment samples in which luminescence signals have not been reset during transport is consistent with debris-flow transport in which grains were only rarely exposed to sunlight. The periodically occurring lenses within the terrace deposits are likely deposits from successive debris flows or surges, or they may represent lateral heterogeneity as the main debris-flow lobes shifted across the floodplain (as is apparent in the modern floodplain). Bull (1991), in contrast, interpreted the angularity of the T7 deposits as derived from frost weathering of bedrock during full-glacial conditions, but that their transport to the streambed by runoff did not occur until the early to mid-Holocene. This model requires stable hillslopes over several thousand years during the late Pleistocene and early Holocene (Bull1, 1991), which we find hard to reconcile with erosion rates of ~1 mm/yr (DiBiase et al., 2010) in this part of the San Gabriel Mountains.

Fourth, we do not observe any significant change in channel slope or grain size between the terrace treads and the modern channel, suggesting no major changes in the transport regime. Grain-size distributions within terraces are similar to those in the active channels and floodplains at very different locations within the drainage, which suggests that the processes transporting sediment through the canyons have remained approximately the same. Although this argument needs to be substantiated with more observations, it would corroborate the hypothesis of a debris-flow origin of both the terrace and the streambed sediments.

Finally, because large parts of the San Gabriel Mountains are mostly bedrock with little hillslope storage of sediment, it is unlikely for small changes in climate to cause large changes in sediment supply. Most debris flows in the San Gabriel Mountains are associated with winter storm events and are particularly common after wildfires (e.g., Doehring, 1968; Lavé and Burbank, 2004; Cannon et al., 2010; Lamb et al., 2011; Kean et al., 2011). There exist numerous historical examples of debris flows that reached urban areas outside of the San Gabriel Mountains (e.g., Chawner, 1935; Morton and Hauser, 2001), and these events were the reason for the construction of debris retention basins fringing the San Gabriel Mountains (LACDPW, 1991). According to current models, loose sediments are stored on steep hillslopes behind vegetation dams (Lamb et al., 2011, 2013). These are frequently destroyed by wildfires, which have recurrence intervals of ~30 yr (DiBiase and Lamb, 2013), and which release the sediment to steep river channels. Ensuing runoff during winter storms evacuates these channels, typically leading to mud and debris flows (Doehring, 1968; Morton and Hauser, 2001; Cannon et al., 2008; Prancevic et al., 2014). The volume of material that can be released from hillslopes is thus limited by the rate of soil production and the size of vegetation dams. Because soil production rates in the San Gabriel Mountains are high (Heimsath et al., 2012), and vegetation dams are rather small, hillslope storage in the San Gabriel Mountains tends to be saturated within decades (Lamb et al., 2011; DiBiase and Lamb, 2013). Therefore, the amount of hillslope material that can be released by environmental changes is strongly limited. Unlike soil-mantled landscapes, in the San Gabriel Mountains there simply is not a large reservoir of colluvium to mine. Moreover, changes in the rate of soil production are likely too small to explain rapid valley aggradation in a few thousand years.

At odds with our bedrock-landscape hypothesis is that of Bull (1991), who suggested that different terraces levels in the North Fork San Gabriel Canyon, in addition to T7, also reflect the impacts of earlier climatic changes. Specifically, the higher-lying T1, T3, and T4 terraces (Figs. 5 and 8) were thought to stem from aggradation-incision cycles during the middle to late Pleistocene (Bull, 1991). The abundance of sediment-mantled strath terraces in the Bear Creek Canyon and the West Fork of the San Gabriel River at similar elevations above the river suggests the possibility that these terraces could have a similar origin. Strath terraces are common in the San Gabriel Mountains and may record an increase in tectonic activity (DiBiase et al., 2015). Unfortunately, we were not able to locate exposures of these terraces to verify if they are fill or strath. While the existence of a T3 terrace is debatable, Bull (1991) observed that the T4 terrace within the North Fork is indeed a fill terrace. Thus, the climate-change hypothesis remains a viable explanation for older terraces in the North Fork San Gabriel River, which deserve targeted future work.

Fill Terrace Formation Caused by Deep-Seated Landslides

Instead of climate change, here we propose that the deep-seated landslides in the upper part of the North Fork San Gabriel Canyon provided the sediment supply that led to valley aggradation, primarily by debris flows, and the formation of terraces. Figure 17 provides a simple sketch of how we think the valley aggradation is related to the deep-seated landslide: (A) First, a more extensive Crystal Lake landslide deposited large amounts of easily erodible material in the headwaters of the North Fork San Gabriel Canyon, probably at ca. 8–9 ka. (B, C) Headward erosion into the landslide deposits triggered abundant debris flows that stacked on top of each other and filled up the valley below the landslide, probably at very high rates. (D) Progressive valley aggradation and erosion of the landslide deposits reduced the relief contrasts and the sediment supply, which eventually caused reincision of the valley fill. In the following paragraphs, we discuss whether this model is consistent with the available data.

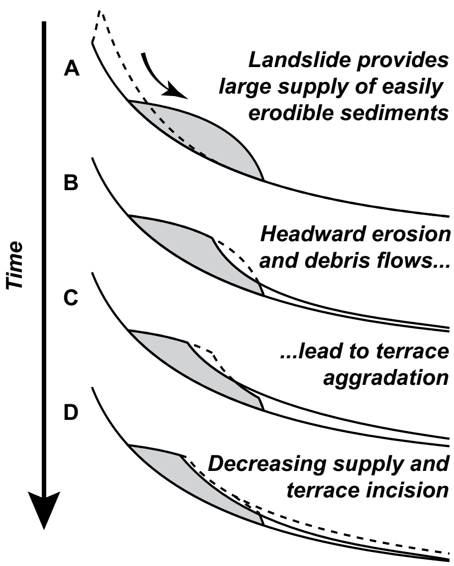

Figure 17. Sketch of fill-terrace formation by debris flows due to sediment supply from a large landslide.

The landslide deposits in the upper part of the North Fork San Gabriel Canyon constitute a huge storage of unconsolidated material that could account for a long-lived source of debris flows. The Wright Mountain landslide (near the town of Wrightwood, ~20 km to the east), for example, formed prior to A.D. 1500, but it is still an ongoing source of debris flows that are frequently triggered by snowmelt and rain (e.g., Morton and Kennedy, 1979). Following the landslide events in the North Fork San Gabriel Canyon, loose sediments without any vegetation cover were exposed to erosion over large areas of the catchment. Subsequent incision of rivers and debris flows into the landslide deposits has probably been rapid, which is supported by the 35 m of incision into the surface of the Alpine Creek landslide in Cloudburst Canyon at an average rate of ~35 mm yr^{-1} during the last ~1000 yr. Even nowadays, the headscarp area of the Alpine Creek landslide is feeding large talus cones at rates that are high enough to prevent colonization by vegetation. Once the landslide surface had been colonized by vegetation, the same principles as on other hillslopes apply, namely, that wildfires and heavy precipitation events increase the chance for debris flows (e.g., Lamb et al., 2011).

In case the initial, more extensive Crystal Lake landslide deposit was truly the source of debris flows that built up the valley fill, our estimated volume of the valley fill would have to be smaller than the landslide deposit. Morton et al. (1989) suggested that the Crystal Lake landslide deposit had a minimum volume of 0.6 km^3, but it is not clear what this estimate was based on. Using a landslide area-volume scaling relationship that is based on a global data set (Volume = $0.146 \pm 0.005 \times \text{Area}^{1.332 \pm 0.005}$; Larsen et al., 2010), and the currently exposed area of the Crystal Lake landslide (~7 km^2), we estimate a volume of 1.95 ± 0.09 km^3. When adding the area of the lowermost landslide deposit (0.4 km^2), near the toe of the Alpine Canyon landslide, the volume estimate increases to 2.1 ± 0.09 km^3. Therefore, the estimated volume of the valley fill (0.1 km^3) could indeed account for the sediments that were eroded from an initial, more extensive Crystal Lake landslide deposit. For comparison, if the entire valley fill were derived from hillslopes upstream of the fill, the equivalent soil/regolith thickness would have to be ~4 m, assuming similar densities. Although this number would be somewhat smaller if part of the valley fill stemmed from older aggradation episodes, soils in the San Gabriel Mountains, if present, have typical depths of less than ~75 cm (Dixon et al., 2012; Heimsath et al., 2012). A hillslope origin of the valley fill would thus require significantly thicker soils in the past, which is difficult to reconcile with the high steepness of the hillslope angles (DiBiase and Lamb, 2013).

Furthermore, if our hypothesis about the origin of the valley fill in the North Fork San Gabriel Canyon is true, the landslide would have to predate the aggradation of the valley fill. Although we obtained only four IRSL sample ages from the aggradational period, these ages are in good agreement with the two ^{14}C ages previously obtained by Bull (1991), and they suggest that between 7 and 8 ka, aggradation of the valley fill was under way. Because the base of the valley fill is currently not exposed, the aggradation phase likely initiated somewhat earlier, but it is difficult to judge by how much. From measurements of sediment yield of the San Gabriel River, we can estimate the time scale for depositing the valley fill. Between 1937 and 2006, the mean annual sediment accumulation behind the San Gabriel Dam was ~580,000 m^3 yr^{-1} (LACDPW, 1991), which is equivalent to a mean basinwide erosion rate in the San Gabriel catchment of ~1 mm yr^{-1}, consistent with detrital ^{10}Be-data from this region (DiBiase et al., 2010). The annual sediment yield from areas upstream of the valley fill (~25 km^2) amounts to ~25,000 m^3 yr^{-1}, and filling up the valley with ~0.1 km^3 of sediment would thus have taken ~4000 yr. These sediment yields, however, correspond to areas that are largely free of landslide material, and it is most likely that sediment yields from the landslide areas have been much higher, resulting in more rapid valley aggradation.

It has been shown previously that sediment yields from recently burned areas are often an order of magnitude higher than the background rates, presumably due to the transition from supply- to transport-limited processes (Doehring, 1968; Lavé and Burbank, 2004; Lamb et al., 2011). If the same logic applies to fresh landslide deposits, where loose sediment is virtually unlimited, the filling could potential occur over a few hundred years. The apparent rapid incision of the Alpine Canyon landslide and the lack of aggradation in Bichota Canyon support our assumption that the landslide material is easier to erode than bedrock. Decadal hillslope erosion rates in the Illgraben, one of the most active debris-flow catchments in the Swiss Alps (Schlunegger et al., 2009), for example, range between ~200 and 400 mm yr^{-1} (Bennett et al., 2012, 2013). Although this catchment contains no large landslide deposit, it is developed in highly fractured metasedimentary rocks that might be considered comparable. Korup et al. (2004) estimated immediate postfailure sediment yields from three large historic landslides in the Southern Alps, New Zealand, to be in excess of 70,000 t km^{-2} yr^{-1}, which translates to erosion rates of ~37 mm yr^{-1} (for an assumed landslide deposit density of 1.9 g cm^{-3}). Decadal-scale erosion rates were on the order of 13–18 mm yr^{-1} and resulted in rapid valley aggradation over a downstream length of >7.5 km (Korup et al., 2004). From these numbers, and our millennial incision rate of the Alpine Canyon landslide deposit, erosion rates of landslide deposits in the North Fork San Gabriel Canyon of >10 mm yr^{-1} appear plausible and would allow filling up the valley in less than ~650–800 yr, for typical trapping efficiencies of ~50%–60% (Korup et al., 2004). Therefore, we conclude that the time frame for valley aggradation postdating the earliest landslide (ca. 8–9 ka) in the North Fork San Gabriel Canyon appears to be reasonable.

In our study, we did not constrain the age of the T7 terrace surface, which we consider the top surface of the postlandslide valley fill. If valley aggradation was truly rapid, reincision of the valley fill might have started soon after ca. 7 ka, probably at a rate that was limited by bedrock incision in the epigenetic gorge. During the downcutting, the formation of multiple cut terraces could occur even in the absence of climatic changes. In this regard, one may wonder if the older terraces, i.e., T1, T4, and perhaps T3, could have been formed in a similar fashion. At this stage, there do not exist enough observations to make a firm conclusion, but the ca. 33 ka boulder age we obtained from near the drainage divide with the Bear Creek may indicate an even older landslide, which could have triggered a similar episode of aggradation and incision that produced the older terraces. It is also possible that these terraces represent cuts into the same landslide-derived fill as the younger ones. The more extensive planation of the T7 surface could then be related to a change in substratum when the river encountered bedrock and formed the epigenetic gorge. Finally, the T1 and T4 terraces could also be strath terraces similar to the ones we observe in the Bear Creek, but according to Bull (1991), at least the T4 terrace consists of alluvium.

Landslide Trigger and Timing

There exist abundant landslide deposits within the San Gabriel Mountains (Morton and Miller, 2006), but the Crystal Lake and Alpine Canyon landslides in the North Fork San Gabriel Canyon are the most extensive ones (Morton et al., 1989). An obvious question is therefore: Do they owe their occurrence to special conditions exclusively found in this valley? Neither the present-day local climate, nor the bedrock geology, or the proximity to active faults like the San Andreas fault, appears sufficiently distinct from the rest of the San Gabriel Mountains to favor large landslides exclusively in the North Fork San Gabriel Canyon. The gentle-sloping terrain in the vicinity of the San Gabriel fault zone (Fig. 2) suggests that tectonically induced fractures act to lower rock mass strength, but there is no obvious fault zone in the upper part of the North Fork San Gabriel Canyon. We note, however, that this canyon lies within a zone of very high relief that stretches from the Bear Creek Canyon eastward across the North Fork San Gabriel Canyon and the Mount Baldy area toward the southeastern edge of the San Gabriel Mountains (Fig. 18). Regions that lie to the northwest of the North Fork San Gabriel and Bear Creek Canyons are relatively high in altitude (>1500 m), but they exhibit lower relief. Cosmogenic-nuclide–derived erosion rates (DiBiase et al., 2010) and mineral

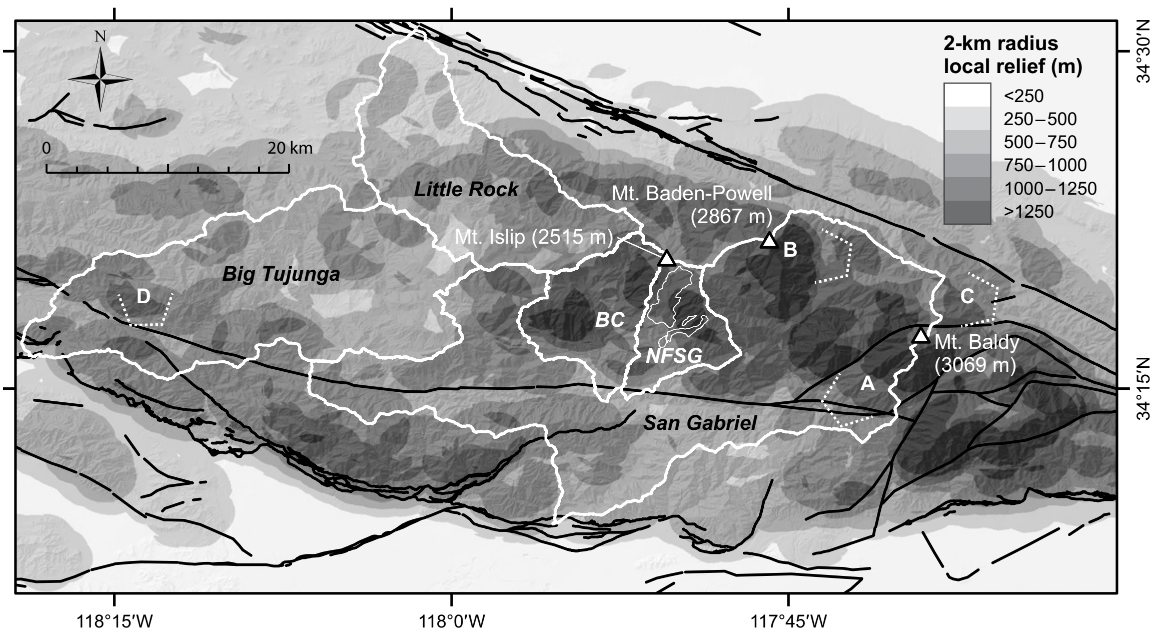

Figure 18. Map of the San Gabriel Mountains showing 2-km-radius local relief (grayscale colors), catchment boundaries (thick white lines), selected mountain peaks (triangles), the landslide deposits in the North Fork San Gabriel Canyon (NFSG; thin white lines), potentially seismogenic faults (black lines), and locations (letters A–D) of debris-flow catchments shown in Figure 19. BC—Bear Creek catchment.

cooling ages (Blythe et al., 2000) record much faster short- and long-term erosion of the high-relief versus the low-relief areas, which implies that headward incision of the San Gabriel drainage maintains or accentuates the relief contrast between these two morphologic domains. As a result, topographically induced stresses in the high-relief area are likely larger than in regions of lower relief (e.g., Miller and Dunne, 1996). It is clear that the Crystal Lake and Alpine Creek landslide deposits have reduced the topographic relief in the headwaters of the North Fork San Gabriel Canyon. In fact, the present-day topography in the headwaters of the Bear Creek Canyon may resemble that of the North Fork San Gabriel Canyon prior to failure. Consequently, the headwaters of Bear Creek Canyon could potentially be sites of future large landslides. It is also conceivable that similar large landslides, of which no more evidence exists, occurred during earlier times in areas of rapid valley incision and high topographic relief.

Periods of wetter climates may trigger large landslides through enhanced pore pressure (e.g., Bookhagen et al., 2005; Dortch et al., 2009; Zerathe et al., 2014). Because past climatic changes in the San Gabriel Mountains are debated, it remains uncertain if they could have affected the timing of landslides in the North Fork San Gabriel Canyon. However, irrespective of potential climatic influences, the proximity of the San Gabriel Mountains to seismogenic faults seems to provide ample opportunities to trigger large slope failures on a frequent basis. Paleoseismic records from Wrightwood indicate recurrence intervals of surface-rupturing earthquakes along the San Andreas fault of ~100 yr over the past 1500 yr (Weldon et al., 2004). Although recurrence interval estimates for other seismogenic faults, like the Sierra Madre–Cucamonga fault zone to the south (Fig. 1A), do not exist, historical ruptures (Lindvall and Rubin, 2008) show their potential for ground acceleration. Hence, we suspect that the topographic conditions in the headwaters of the North Fork San Gabriel Canyon were the primary factors for the occurrence of exceptionally large landslides, while seismic shaking may have been the actual trigger.

Implications for Landscape Evolution in the San Gabriel Mountains

Our study has shown that the North Fork San Gabriel Canyon has been in a state of topographic disequilibrium since at least ca. 8–9 ka. The lower part of the North Fork San Gabriel Canyon may have been filled with sediments by ca. 6–7 ka, followed by incision. The fact that likely >60% of the valley fill has not yet been excavated suggests that it may take another ~10,000 yr before the North Fork San Gabriel River reaches bedrock again, probably regulated by the rate of river incision within the epigenetic gorge near the confluence with the West Fork of the San Gabriel River. Although incision into the landslide deposits appears to proceed very rapidly, the sheer volume of the landslide deposit is sufficient to keep the upper part of the North Fork San Gabriel Canyon in a transient state for many thousand years to come. This circumstance may also explain part of the scatter that is seen in functional relationships between topographic metrics, such as channel steepness or local relief, and rates of erosion estimated from thermochronology (Spotila et al., 2002) or cosmogenic nuclides (DiBiase et al., 2010).

There exist other catchments in the San Gabriel Mountains where debris flows frequently occur and where the valley has been buried by considerable amounts of sediments (Fig. 19). Examples include active debris-flow catchments on the southwestern slope of Mount Baldy (Fig. 19A), or to the east of Mount Baden-Powell (Fig. 19B). There also exist catchments where deposits with debris-flow channels on the surface provide evidence for past debris-flow activity (Fig. 19C). A tributary of the Big Tujunga River features voluminous deposits that have already been incised again (Fig. 19D). Similar to the North Fork San Gabriel Canyon, these fill deposits are in contrast to widespread strath terraces in the main stem of the Big Tujunga Canyon (DiBiase et al., 2015). These examples indicate that valley aggradation by debris flows may in fact be a frequent process that affects higher-order drainages in the San Gabriel Mountains, and they provide another indication of topographic and erosional disequilibrium.

Implications for Climate Change Impacts in Rapidly Eroding Bedrock Landscapes

Our study has shown that concepts of how hillslopes and rivers respond to climate change that are largely based on landscapes with thick soil mantles (e.g., Bull, 1991) may not apply to steep, and rapidly eroding arid bedrock landscapes. Although river terraces have proven to be useful indicators of climate change in glaciated and soil-mantled landscapes (e.g., Knox, 1983; Bull, 1991; Bridgland and Westaway, 2008; Pazzaglia, 2013), there currently exists little evidence that they form in a similar fashion in the San Gabriel Mountains. We think that this is partly related to the limited amount of hillslope sediment that can be stored in these environments. Although prolonged periods of more humid conditions could allow for changing types of vegetation cover and therefore damming capacities, this only leads to increasing hillslope storage if wildfires do not destroy these dams on a regular basis as they do now, and if soil production rates are higher than river incision rates. Heimsath et al. (2012) reported soil production rates in the San Gabriel Mountains of up to ~0.5 mm yr^{-1}, but rates higher than ~0.2 mm yr^{-1} only occur on hillslopes steeper than 30°, with thin (<30 cm) and patchy soil cover that is frequently stripped off by landslides (Heimsath et al., 2012; DiBiase et al., 2012).

Although soil production rates may increase with precipitation, observations indicate that this holds only for low erosion rates (<0.05 mm yr^{-1}; Dere et al., 2013) and is more pronounced under arid to hyperarid conditions (mean annual precipitation <100 mm yr^{-1}; Owen et al., 2011). Therefore, even if climatic changes in the San Gabriel Mountains would cause markedly more humid conditions, the ability to accumulate significant amounts of sediment on hillslopes appears limited, mainly because they are rapidly uplifting and steeper than the angle of repose (e.g., Lamb et al., 2011; DiBiase et al., 2012). A fundamental transition from bedrock to soil-covered hillslopes would thus require lower hillslope angles. However, erosion rates from decades to thousands of years and millions of years show no major changes (Blythe et al., 2000; Spotila et al., 2002; Lavé and Burbank, 2004; DiBiase et al., 2010; Lamb et al., 2011), and landscape adjustment time scales to changes in uplift rate in the San Gabriel Mountains play out over a few million years (DiBiase et al., 2015).

Loose sediment may also accumulate in colluvial hollows before it enters the valley network (e.g., Reneau et al., 1990). However, in the San Gabriel Mountains, colluvial hollows are typically scoured by debris flows that are frequently triggered by winter storms and are particularly common after wildfires (e.g., Kean et al., 2011). Furthermore, our work and previous studies (Stock and Dietrich, 2003, 2006) suggest that considerable parts of the San Gabriel Mountains are shaped by debris flows, and it is also not clear how debris-flow channels respond to changes in sediment supply and water discharge. Together, these unknowns make it difficult to determine the response of steep, unglaciated bedrock landscapes to climate change. It is clear, however, that lessons learned from glaciated, fluvial-dominated, and soil-mantled landscapes may not simply translate to steep bedrock landscapes.

CONCLUSION

The North Fork San Gabriel Canyon is an arid, rapidly eroding, bedrock landscape in the San Gabriel Mountains, California, that fea-

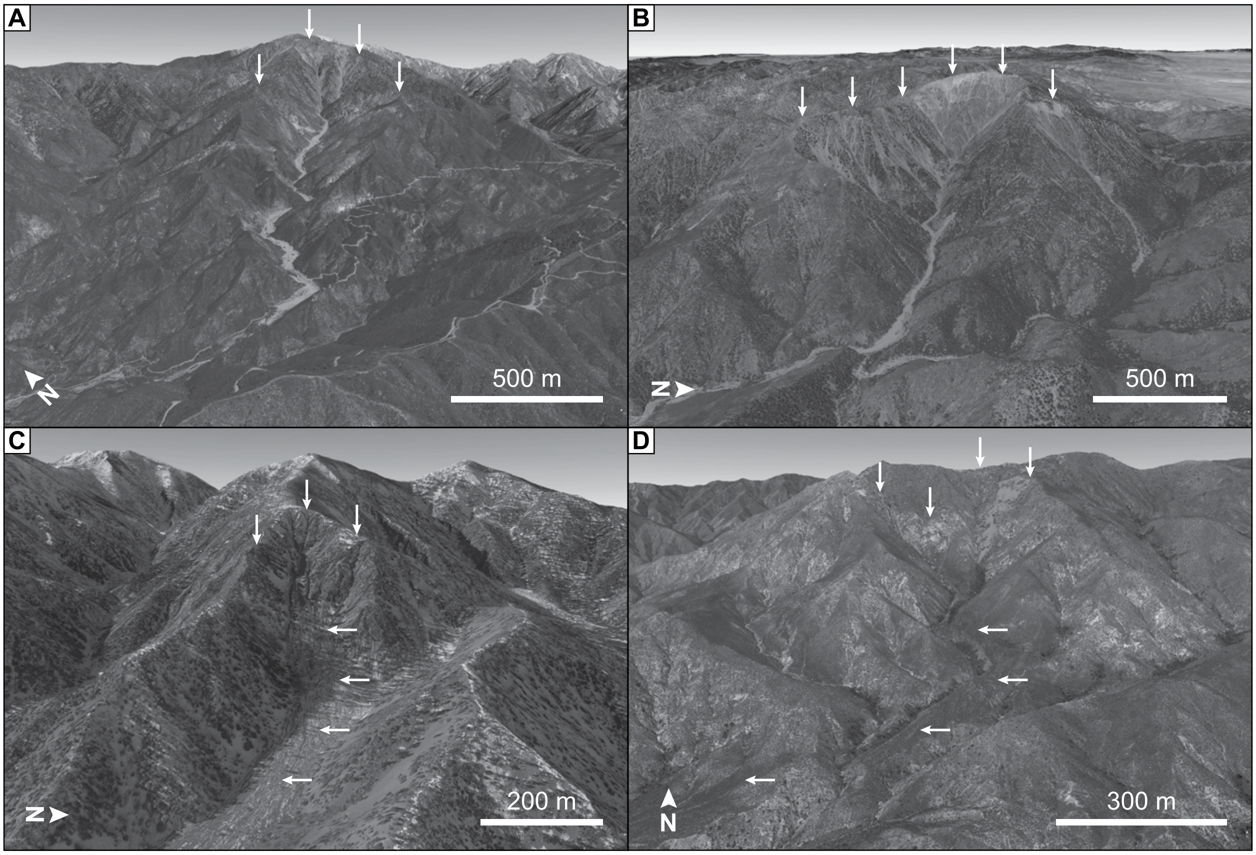

Figure 19. (dashed lines indicate viewing direction) Oblique aerial views of active (A, B) and inactive (C, D) debris-flow catchments in the San Gabriel Mountains. Vertical arrows indicate sediment source areas; horizontal arrows indicate debris-flow deposits. Distance from source area to toe of debris-flow deposits is ~9 km (A), 4 km (B), 2 km (C), and 4 km (D). All images are from Google Earth.

tures a series of prominent fill terraces that were previously related to periods of river aggradation induced by climatic changes (Bull, 1991). We challenge this view and instead propose that deep-seated landslides in the upper part of the North Fork San Gabriel Canyon provided voluminous sediment supply that led to valley aggradation, primarily by debris flows, and the formation of terraces. A debris-flow origin of the terrace deposits is supported by our morphological and sedimentological observations, and the scarcity of grains that were exposed to sunlight long enough to completely bleach their luminescence signal, and it is consistent with abundant debris-flow deposits throughout the San Gabriel Mountains. Our new Holocene exposure ages reveal that the Crystal Lake and Alpine Canyon landslides are much younger than previously assumed, and that subsequent erosion of the landslide material was very rapid. The debris-flow origin of the terrace deposits renders accurate dating of the aggradation period by luminescence methods difficult, but our new ages based on post-IR IRSL single-grain dating are consistent with available ^{14}C ages and indicate that aggradation occurred during the early-mid-Holocene, subsequent to the oldest landslide event. The occurrence of these landslides in the North Fork San Gabriel Canyon is probably promoted by large topographic stresses associated to high landscape relief, and proximity to seismogenic faults like the San Andreas Fault.

These results show that enhanced sediment supply following large deep-seated landslides can produce valley fills and terraces that resemble fluvial terraces, especially when the debris-flow deposits are fluvially reworked, but they may have origins independent of climate change. In fact, the lack of a continuous soil cover and the limited storage of hillslope sediments in steep and arid bedrock landscapes appear to greatly limit the potential for climatic changes to cause significant valley aggradation by fluvial deposition. Furthermore, our study has shown that erosion and sediment transport processes in the San Gabriel Mountains can be highly episodic in space and time, and interspersed with aggradational periods. These circumstances create ambiguity in the interpretation of erosion rate estimates that integrate over time scales of less than 10^4 yr and relationships between landscape-scale erosion rates and morphometric parameters.

ACKNOWLEDGMENTS

This project was supported by the Gordon and Betty Moore Foundation, through the Tectonics Observatory, National Science Foundation grant EAR-0838495. Scherler was supported by a Feodor Lynen Scholarship through the Alexander von Humboldt Foundation. Lamb acknowledges support from the donors of the American Chemical Society Petroleum Research Fund. We thank two anonymous reviewers and the Associate Editor F. Pazzaglia for constructive comments that helped improving the paper. This work started as a Caltech class project, and we are thankful for help from the participants of Ge125.

REFERENCES CITED

Armitage, J.J., Duller, R.A., Whittaker, A.C., and Allen, P.A., 2011, Transformation of tectonic and climatic signals from source to sedimentary archive: Nature Geoscience, v. 4, p. 231–235, doi:10.1038/ngeo1087.

Balco, G., Stone, J., Lifton, N., and Dunai, T., 2008, A complete and easily accessible means of calculating

surface exposure ages or erosion rates from ^{10}Be and ^{26}Al measurements: Quaternary Geochronology, v. 3, p. 174–195, doi:10.1016/j.quageo.2007.12.001.
Behr, W.M., Rood, D.H., Fletcher, K.E., Guzman, N., Finkel, R., Hanks, T.C., Hudnut, K.W., Kendrick, K.J., Platt, J.P., Sharp, W.D., Weldon, R.J., and Yule, J.D., 2010, Uncertainties in slip-rate estimates for the Mission Creek strand of the southern San Andreas fault at Biskra Palms Oasis, Southern California: Geological Society of America Bulletin, v. 122, p. 1360–1377, doi:10.1130/B30020.1.
Bennett, G.L., Molnar, P., Eisenbeiss, H., and McArdell, B.W., 2012, Erosional power in the Swiss Alps: Characterization of slope failure in the Illgraben: Earth Surface Processes and Landforms, v. 37, p. 1627–1640, doi:10.1002/esp.3263.
Bennett, G.L., Molnar, P., McArdell, B.W., Schlunegger, F., and Burlando, P., 2013, Patterns and controls of sediment production, transfer and yield in the Illgraben: Geomorphology, v. 188, p. 68–82, doi:10.1016/j.geomorph.2012.11.029.
Blum, M.D., and Törnqvist, T.E., 2000, Fluvial responses to climate and sea-level change: A review and look forward: Sedimentology, v. 47, p. 2–48, doi:10.1046/j.1365-3091.2000.00008.x.
Blythe, A.E., Burbank, D.W., Farley, K.A., and Fielding, E.J., 2000, Structural and topographic evolution of the central Transverse Ranges, California, from apatite fission-track, (U-Th)/He and digital elevation model analyses: Basin Research, v. 12, p. 97–114, doi:10.1046/j.1365-2117.2000.00116.x.
Blythe, A.E., House, M.A., and Spotila, J.A., 2002, Low-temperature thermochronology of the San Gabriel and San Bernardino Mountains, Southern California: Constraining structural evolution, *in* Barth, A., ed., Contributions to Crustal Evolution of the Southwestern United States: Geological Society of America Special Paper 365, p. 231–250, doi:10.1130/0-8137-2365-5.231.
Bookhagen, B., Thiede, R.C., and Strecker, M.R., 2005, Late Quaternary intensified monsoon phases control landscape evolution in the northwest Himalaya: Geology, v. 33, no. 2, p. 149–152, doi:10.1130/G20982.1.
Brakenridge, G.R., 1980, Widespread episodes of stream erosion during the Holocene and their climatic cause: Nature, v. 283, p. 655–656, doi:10.1038/283655a0.
Bridgland, D., and Westaway, R., 2008, Climatically controlled river terrace staircases: A worldwide Quaternary phenomenon: Quaternary Science Reviews, v. 98, p. 285–315.
Bull, W.B., 1979, Threshold of critical power of streams: Geological Society of America Bulletin, v. 90, p. 453–464, doi:10.1130/0016-7606(1979)90<453:TOCPIS>2.0.CO;2.
Bull, W.B., 1991, Geomorphic Responses to Climatic Change: New York, Oxford University Press, 352 p.
Cannon, S.H., Boldt, E.M., Kean, J.W., Laber, J.L., and Staley, D.M., 2010, Relations Between Rainfall and Postfire Debris-Flow and Flood Magnitudes for Emergency-Response Planning, San Gabriel Mountains, Southern California: U.S. Geological Survey Open-File Report 2010–1039, 31 p.
Cannon, S.H., Gartner, J.E., Wilson, R.C., Bowers, J.C., and Laber, J.L., 2008, Storm rainfall conditions for floods and debris flows from recently burned areas in southwestern Colorado and Southern California: Geomorphology, v. 96, p. 250–269, doi:10.1016/j.geomorph.2007.03.019.
Chawner, W.D., 1935, Alluvial fan flooding: The Montrose, California, flood of 1934: Geographical Review, v. 25, p. 255–263, doi:10.2307/209600.
Crook, R., Jr., 1986, Relative dating of Quaternary deposits based on P-wave velocities in weathered granitic clasts: Quaternary Research, v. 25, p. 281–292, doi:10.1016/0033-5894(86)90002-5.
Davis, W.M., 1909, Geographical Essays: New York, Dover Publications, 777 p.
Dere, A.L., White, T.S., April, R.H., Reynolds, B., Miller, T.E., Knapp, E.P., McKay, L.D., and Brantles, S.L., 2013, Climate dependence of feldspar weathering in shale soils along a latitudinal gradient: Geochimica et Cosmochimica Acta, v. 122, p. 101–126, doi:10.1016/j.gca.2013.08.001.
DiBiase, R.A., 2011, Tectonic Geomorphology of the San Gabriel Mountains, CA [Ph.D. thesis]: Tempe, Arizona, Arizona State University, 247 p.
DiBiase, R.A., and Lamb, M.P., 2013, Vegetation and wildfire controls on sediment yield in bedrock landscapes: Geophysical Research Letters, v. 40, p. 1093–1097, doi:10.1002/grl.50277.
DiBiase, R.A., and Whipple, K.X., 2011, The influence of erosion thresholds and runoff variability on the relationships among topography, climate, and erosion rate: Journal of Geophysical Research, v. 116, p. F04036, doi:10.1029/2011JF002095.
DiBiase, R.A., Whipple, K.X., Lamb, M.P., and Heimsath, A.M., 2015, The role of waterfalls and knick zones in controlling the style and pace of landscape adjustment in the western San Gabriel Mountains, California: Geological Society of America Bulletin, v. 127, p. 539–559, doi:10.1130/B31113.1.
DiBiase, R.A., Whipple, K.X., Heimsath, A.M., and Ouimet, W.B., 2010, Landscape form and millennial erosion rates in the San Gabriel Mountains, CA: Earth and Planetary Science Letters, v. 289, no. 1–2, p. 134–144, doi:10.1016/j.epsl.2009.10.036.
DiBiase, R.A., Heimsath, A.M., and Whipple, K.X., 2012, Hillslope response to tectonic forcing in threshold landscapes: Earth Surface Processes and Landforms, v. 37, p. 855–865, doi:10.1002/esp.3205.
Dixon, J.L., Hartshorn, A.S., Heimsath, A.M., DiBiase, R.A., and Whipple, K.X., 2012, Chemical weathering response to tectonic forcing: A soils perspective from the San Gabriel Mountains, California: Earth and Planetary Science Letters, v. 323–324, p. 40–49.
Doehring, D.O., 1968, The effect of fire on geomorphic processes in the San Gabriel Mountains, California: Wyoming University Contributions to Geology, v. 7, p. 43–65.
Dortch, J.M., Owen, L.A., Haneberg, W.C., Caffee, M.C., Dietsch, C., and Kamp, U., 2009, Nature and timing of large landslides in the Himalaya and Transhimalaya of northern India: Quaternary Science Reviews, v. 28, p. 1037–1054, doi:10.1016/j.quascirev.2008.05.002.
Dunne, J., Elmore, D., and Muzikar, P., 1999, Scaling factors for the rates of production of cosmogenic nuclides for geometric shielding and attenuation at depth on sloped surfaces: Geomorphology, v. 27, p. 3–11, doi:10.1016/S0169-555X(98)00086-5.
Eaton, E.C., 1935, Flood and erosion control problems and their solution: American Society of Civil Engineers Transactions, v. 101, p. 1302–1330.
Finnegan, N.J., and Dietrich, W.E., 2011, Episodic bedrock strath terrace formation due to meander migration and cutoff: Geology, v. 39, no. 2, p. 143–146.
Fletcher, K.E.K., Sharp, W.D., Kendrick, K.J., Behr, W.M., Hudnut, K.W., and Hanks, T., 2010, ^{230}Th/U dating of a late Pleistocene alluvial fan along the southern San Andreas fault: Geological Society of America Bulletin, v. 122, p. 1347–1359, doi:10.1130/B30018.1.
Flint, J.J., 1974, Stream gradient as a function of order, magnitude, and discharge: Water Resources Research, v. 10, p. 969–973, doi:10.1029/WR010i005p00969.
Hack, J.T., 1957, Studies of Longitudinal Stream Profiles in Virginia and Maryland: U.S. Geological Survey Professional Paper 294-B, 97 p.
Heimsath, A.M., DiBiase, R.A., and Whipple, K.X., 2012, Soil production limits and the transition to bedrock-dominated landscapes: Nature Geoscience, v. 5, no. 3, p. 210–214, doi:10.1038/ngeo1380.
Jennings, C.W., and Bryant, W.A., 2010, Fault Activity Map of California: California Geological Survey Geologic Data Map 6, scale 1:750,000.
Kean, J.W., Staley, D.M., and Cannon, S.H., 2011, In situ measurements of post-fire debris flows in Southern California: Comparisons of the timing and magnitude of 24 debris-flow events with rainfall and soil moisture conditions: Journal of Geophysical Research, v. 116, p. F04019, doi:10.1029/2011JF002005.
Kean, J.W., McCoy, S.W., Tucker, G.E., Staley, D.M., and Coe, J.A., 2013, Runoff-generated debris flows: Observations and modeling of surge initiation, magnitude, and frequency: Journal of Geophysical Research–Earth Surface, v. 118, p. 2190–2207, doi:10.1002/jgrf.20148.
Kirby, E., and Whipple, K.X., 2012, Expression of active tectonics in erosional landscapes: Journal of Structural Geology, v. 44, p. 54–75, doi:10.1016/j.jsg.2012.07.009.
Kirby, M.E., Lund, S.P., Anderson, M.A., and Bird, B.W., 2007, Insolation forcing of Holocene climate change in Southern California: A sediment study from Lake Elsinore: Journal of Paleolimnology, v. 38, p. 395–417, doi:10.1007/s10933-006-9085-7.
Knox, J.C., 1983, Responses of river systems to Holocene climates, *in* Wright, H.E., Jr., ed., Late Quaternary Environments of the United States: Volume 2. The Holocene: Minneapolis, Minnesota, University of Minnesota Press, p. 26–41.
Korup, O., McSaveney, M.J., and Davies, T.R.H., 2004, Sediment generation and delivery from large historic landslides in the Southern Alps, New Zealand: Geomorphology, v. 61, p. 189–207, doi:10.1016/j.geomorph.2004.01.001.
Korup, O., Strom, A.L., and Weidinger, J.T., 2006, Fluvial response to large rock-slope failures: Examples from the Himalayas, the Tien Shan, and the Southern Alps in New Zealand: Geomorphology, v. 78, p. 3–21, doi:10.1016/j.geomorph.2006.01.020.
Lal, D., 1991, Cosmic-ray labeling of erosion surfaces: In situ nuclide production-rates and erosion models: Earth and Planetary Science Letters, v. 104, no. 2–4, p. 424–439, doi:10.1016/0012-821X(91)90220-C.
Lamb, M.P., Scheingross, J.S., Amidon, W.H., Swanson, E., and Limaye, A., 2011, A model for fire-induced sediment yield by dry ravel in steep landscapes: Journal of Geophysical Research, v. 116, p. F03006, doi:10.1029/2010JF001878.
Lamb, M.P., Levina, M., DiBiase, R.A., and Fuller, B., 2013, Sediment storage by vegetation in steep bedrock landscapes: Theory, experiments, and implications for postfire sediment yield: Journal of Geophysical Research, v. 118, p. 1147–1160, doi:10.1002/jgrf.20058.
Lane, E.W., 1955, The importance of fluvial morphology in hydraulic engineering: American Society of Civil Engineers Proceedings Separate, v. 81, no. 745, p. 1–17.
Larsen, I.J., Montgomery, D.R., and Korup, O., 2010, Landslide erosion controlled by hillslope material: Nature Geoscience, v. 3, p. 247–251, doi:10.1038/ngeo776.
Lavé, J., and Avouac, J.-P., 2001, Fluvial incision and tectonic uplift across the Himalayas of central Nepal: Journal of Geophysical Research, v. 106, no. B12, p. 26,561–26,591, doi:10.1029/2001JB000359.
Lavé, J., and Burbank, D., 2004, Denudation processes and rates in the Transverse Ranges, Southern California: Erosional response of a transitional landscape to external and anthropogenic forcing: Journal of Geophysical Research–Earth Surface, v. 109, p. F01006, doi:10.1029/2003jf000023.
Leopold, L.B., Wolman, M.G., and Miller, J.P., 1964, Fluvial Processes in Geomorphology: San Francisco, California, W.H. Freeman and Co., 522 p.
Limaye, A.B.S., and Lamb, M.P., 2014, Numerical simulations of bedrock valley evolution by meandering rivers with variable bank material: Journal of Geophysical Research, v. 119, p. 927–950, doi:10.1002/2013JF002997.
Lindvall, S.C., and Rubin, C.M., 2008, Slip Rate Studies along the Sierra Madre–Cucamonga Fault System Using Geomorphic and Cosmogenic Surface Exposure Age Constraints: Collaborative Research with Central Washington University and William Lettis & Associates, Inc.: U.S. Geological Survey Final Report 03HQGR0084, 13 p.
Los Angeles County Department of Public Works (LACDPW), 2006, Hydrology Manual, Reference Guide: Los Angeles, California, LACDPW, 160 .
Mackin, J.H., 1948, Concept of the graded river: Geological Society of America Bulletin, v. 101, p. 1373–1388.
Matmon, A., Schwartz, D.P., Finkel, R., Clemmens, S., and Hanks, T., 2005, Dating offset fans along the Mojave section of the San Andreas fault using cosmogenic ^{26}Al and ^{10}Be: Geological Society of America Bulletin, v. 117, p. 795–807, doi:10.1130/B25590.1.
Matti, J.C., and Morton, D.M., 1993, Paleogeographic evolution of the San Andreas fault in Southern California: A reconstruction based on a new cross-fault correlation, *in* Powell, R.E., et al., eds., The San Andreas Fault System, Displacement Palinspastic Reconstruction, and

Geologic Evolution: Geological Society of America Memoir 178, p. 107–159, doi:10.1130/MEM178-p107.

McFadden, L.D., and Weldon, R.J., II, 1987, Rates and processes of soil development on Quaternary terraces in Cajon Pass, California: Geological Society of America Bulletin, v. 98, p. 280–293, doi:10.1130/0016-7606(1987)98<280:RAPOSD>2.0.CO;2.

McGill, S.F., Owen, L.A., Weldon, R.J., II, and Kendrick, K.J., 2013, Latest Pleistocene and Holocene slip rate for the San Bernardino strand of the San Andreas fault, Plunge Creek, Southern California: Implications for strain partitioning within the southern San Andreas fault system for the last ~35 k.y.: Geological Society of America Bulletin, v. 125, p. 48–72, doi:10.1130/B30647.1.

Merritts, D.J., Vincent, K.R., and Wohl, E.E., 1994, Long river profiles, tectonism, and eustasy: A guide to interpreting fluvial terraces: Journal of Geophysical Research, v. 99, p. 14,031–14,050, doi:10.1029/94JB00857.

Miller, D.J., and Dunne, T., 1996, Topographic perturbations of regional stresses and consequent bedrock fracturing: Journal of Geophysical Research, v. 101, no. B11, p. 25,523–25,536, doi:10.1029/96JB02531.

Miller, W.J., 1926, Glaciation in the San Gabriel Mountains, California: The Journal of Geology, v. 34, no. 1, p. 74–82, doi:10.1086/623274.

Molnar, P., Anderson, R.S., Kier, G., and Rose, J., 2006, Relationships among probability distributions of stream discharges in floods, climate, bed load transport, and river incision: Journal of Geophysical Research, v. 111, p. F02001, doi:10.1029/2005JF000310.

Montgomery, D.R., Hallet, B., Yuping, L., Finnegan, N., Anders, A., Gillespie, A., and Greenberg, H.M., 2004, Evidence for Holocene megafloods down the Tsangpo River gorge, southeastern Tibet: Quaternary Research, v. 62, p. 201–207, doi:10.1016/j.yqres.2004.06.008.

Morton, D.M., and Hauser, R.M., 2001, A Debris Avalanche at Forest Falls, San Bernardino County, California, July 11, 1999: U.S. Geological Survey Open-File Report 2001–146, Version 1.0, 67 p.

Morton, D.M., and Miller, F.K., 2006, Geologic Map of the San Bernardino and Santa Ana 30′ × 60′ Quadrangles, California: U.S. Geological Survey Open-File Report 2006–1217, Version 1.0, scale 1:100,000.

Morton, D.M., and Kennedy, M.P., 1979, Part 2: Wright Mountain mudflows—Spring 1969 landsliding: California Division of Mines and Geology Special Report 136, p. 1–6.

Morton, D.M., Sadler, P.M., and Minnich, R.A., 1989, Large rock-avalanche deposits: Examples from the central and eastern San Gabriel Mountains of Southern California, *in* Sadler, P.M., and Morton, D.M., eds., Landslides in a Semi-Arid Environment with Emphasis on the Inland Valleys of Southern California: Inland Geological Society Publication 2, p. 323–337.

National Research Council, 2010, Landscapes on the Edge: Washington, D.C., National Academies Press, 180 p.

Nishiizumi, K., Imamura, M., Caffee, M.C., Southon, J.R., Finkel, R.C., and McAninch, J., 2007, Absolute calibration of ^{10}Be AMS standards: Nuclear Instruments & Methods in Physics Research, section B, Beam Interactions with Materials and Atoms, v. 258, p. 403–413, doi:10.1016/j.nimb.2007.01.297.

Ouimet, W.B., Whipple, K.X., Crsoby, B.T., Johnson, J.P., and Schildgen, T.F., 2008, Epigenetic gorges in fluvial landscapes: Earth Surface Processes and Landforms, v. 33, p. 1993–2009, doi:10.1002/esp.1650.

Owen, J.J., Amundson, R., Dietrich, W.E., Nishiizumi, K., Sutter, B., and Chong, G., 2011, The sensitivity of hillslope bedrock erosion to precipitation: Earth Surface Processes and Landforms, v. 36, p. 117–135, doi:10.1002/esp.2083.

Owen, L.A., Finkel, R.C., Minnich, R.A., and Perez, A.E., 2003, Extreme southwestern margin of late Quaternary glaciation in North America: Timing and controls: Geology, v. 31, no. 8, p. 729–732, doi:10.1130/G19561.1.

Owen, L.A., Clemmens, S.J., Finkel, R.C., and Gray, H., 2014, Late Quaternary alluvial fans at the eastern end of the San Bernardino Mountains, Southern California: Quaternary Science Reviews, v. 87, p. 114–134, doi:10.1016/j.quascirev.2014.01.003.

Parker, G., and Klingeman, P.C., 1982, On why gravel bed streams are paved: Water Resources Research, v. 18, no. 5, p. 1409–1423, doi:10.1029/WR018i005p01409.

Pazzaglia, F.J., 2013, Fluvial terraces, *in* Shroder, J., and Wohl, E., eds., Treatise on Geomorphology: Volume 9. Fluvial Geomorphology: San Diego, California, Academic Press, p. 379–412, doi:10.1016/B978-0-12-374739-6.00248-7.

Pazzaglia, F.J., and Brandon, M.T., 2001, A fluvial record of long-term steady-state uplift and erosion across the Cascadia forearc high, western Washington State: American Journal of Science, v. 301, p. 385–431, doi:10.2475/ajs.301.4-5.385.

Perron, J.T., and Royden, L., 2012, An integral approach to bedrock river profile analysis: Earth Surface Processes and Landforms, v. 38, p. 570–576, doi:10.1002/esp.3302.

Petersen, M.D., and Wesnousky, S.G., 1994, Fault slip rates and earthquake histories for active faults in Southern California: Bulletin of the Seismological Society of America, v. 84, p. 1608–1649.

Poisson, B., and Avouac, J.-P., 2004, Holocene hydrological changes inferred from alluvial stream entrenchment in North Tian Shan (northwestern China): The Journal of Geology, v. 112, no. 2, p. 231–249, doi:10.1086/381659.

Porter, S.C., Zhisheng, A., and Hongbo, Z., 1992, Cyclic Quaternary alluviation and terracing in a nonglaciated drainage basin on the north flank of the Qinling Shan, central China: Quaternary Research, v. 38, p. 157–169, doi:10.1016/0033-5894(92)90053-L.

Prancevic, J., Lamb, M.P., and Fuller, B., 2014, Initial sediment transport across the river-debris flow transition: Geology, v. 42, no. 3, p. 191–194, doi:10.1130/G34927.1.

Reneau, S.L., Dietrich, W.E., Donahue, D.J., Jull, A.J.T., and Ribun, M., 1990, Late Quaternary history of colluvial deposition and erosion in hollows, central California Coast Ranges: Geological Society of America Bulletin, v. 102, p. 969–982, doi:10.1130/0016-7606(1990)102<0969:LQHOCD>2.3.CO;2.

Rhodes, E.J., 2011, Optically stimulated luminescence dating of sediments over the past 200,000 years: Annual Review of Earth and Planetary Sciences, v. 39, p. 461–488, doi:10.1146/annurev-earth-040610-133425.

Rhodes, E.J., 2015, Dating sediments using potassium feldspar single-grain IRSL: Initial methodological considerations: Quaternary International, v. 362, p. 14–22, doi:10.1016/j.quaint.2014.12.012.

Riebe, C.S., Kirchner, J.W., Granger, D.E., and Finkel, R.C., 2001, Minimal climatic control on erosion rates in the Sierra Nevada, California: Geology, v. 29, p. 447–450, doi:10.1130/0091-7613(2001)029<0447:MCCOER>2.0.CO;2.

Roberts, R.G., Galbraith, R.F., Olley, J.M., Laslett, G.M., Yoshida, H., 1999, Optical dating of single grains of quartz from Jinmium rock shelter, Northern Australia. Part II: results, interpretations and implications: Archaeometry, v. 41, p. 365–395.

Scherler, D., Munack, H., Mey, J., Eugster, P., Wittmann, H., Codilean, A.T., Kubik, P., and Strecker, M.R., 2014, Ice dams, outburst floods, and glacial incision at the western margin of the Tibetan Plateau: A >100 k.y. chronology from the Shyok Valley, Karakoram: Geological Society of America Bulletin, v. 126, no. 5–6, p. 738–758, doi:10.1130/B30942.1.

Scherler, D., Bookhagen, B., Wulf, H., Preusser, F., and Strecker, M.R., 2015, Increased late Pleistocene erosion rates during fluvial aggradation in the Garhwal Himalaya, northern India: Earth and Planetary Science Letters, v. 428, p. 255–266, doi:10.1016/j.epsl.2015.06.034.

Schlunegger, F., Badoux, A., McArdell, B.W., Gwerder, C., Schnydrig, D., Rieke-Zapp, D., and Molnar, P., 2009, Limits of sediment transfer in an alpine debris-flow catchment, Illgraben, Switzerland: Quaternary Science Reviews, v. 28, p. 1097–1105, doi:10.1016/j.quascirev.2008.10.025.

Schwanghart, W., and Scherler, D., 2014, Short Communication: TopoToolbox 2—MATLAB-based software for topographic analysis and modeling in Earth surface sciences: Earth Surface Dynamics, v. 2, p. 1–7, doi:10.5194/esurf-2-1-2014.

Sharp, R.P., Allen, C.R., and Meier, M.F., 1959, Pleistocene glaciers on Southern California mountains: American Journal of Science, v. 257, p. 81–94, doi:10.2475/ajs.257.2.81.

Spotila, J.A., House, M.A., Blythe, A.E., Niemi, N.A., and Bank, G.C., 2002, Controls on erosion and geomorphic evolution of the San Bernardino and San Gabriel Mountains, Southern California, *in* Barth, A., ed., Contributions to Crustal Evolution of the Southwestern United States: Geological Society of America Special Paper 365, p. 205–230, doi:10.1130/0-8137-2365-5.205.

Stock, J.D., and Dietrich, W.E., 2003, Valley incision by debris flows: Evidence of a topographic signature: Water Resources Research, v. 39, p. 1089, doi:10.1029/2001WR001057.

Stock, J.D., and Dietrich, W.E., 2006, Erosion of steepland valleys by debris flows: Geological Society of America Bulletin, v. 118, no. 9/10, p. 1125–1148, doi:10.1130/B25902.1.

Stone, J.O., 2000, Air pressure and cosmogenic isotope production: Journal of Geophysical Research, v. 105, p. 23,753–23,759, doi:10.1029/2000JB900181.

Takahashi, T., 2014, Debris Flow: Mechanics, Prediction and Countermeasures (2nd ed.): Boca Raton, Florida, CRC Press, 572 p., doi:10.1201/b16647.

Tchakerian, V.P., and Lancaster, N., 2002, Late Quaternary arid/humid cycles in the Mojave Desert and western Great Basin of North America: Quaternary Science Reviews, v. 21, p. 799–810, doi:10.1016/S0277-3791(01)00128-7.

Van der Woerd, J., Klinger, Y., Sieh, K., Tapponnier, P., Ryerson, F.J., and Mériaux, A.-S., 2006, Long-term slip rate of the southern San Andreas fault from ^{10}Be-^{26}Al surface exposure dating of an offset alluvial fan: Journal of Geophysical Research, v. 111, p. B04407, doi:10.1029/2004JB003559.

Weldon, R.J., II, 1986, The Late Cenozoic Geology of Cajon Pass; Implications for Tectonics and Sedimentation along the San Andreas Fault [Ph.D. thesis]: Pasadena, California, California Institute of Technology, 425 p.

Weldon, R.J., II, and Sieh, K.E., 1985, Holocene rate of slip and tentative recurrence interval for large earthquakes on the San Andreas fault, Cajon Pass, Southern California: Geological Society of America Bulletin, v. 96, p. 793–812, doi:10.1130/0016-7606(1985)96<793:HROSAT>2.0.CO;2.

Weldon, R.J., II, Scharer, K., Fumal, T., and Biasi, G., 2004, Wrightwood and the earthquake cycle: What a long recurrence record tells us about how faults work: GSA Today, v. 14, no. 9, p. 4–10, doi:10.1130/1052-5173(2004)014<4:WATECW>2.0.CO;2.

Whipple, K.X., and Dunne, T., 1992, The influence of debris-flow rheology on fan morphology, Owens Valley, California: Geological Society of America Bulletin, v. 104, p. 887–900, doi:10.1130/0016-7606(1992)104<0887:TIODFR>2.3.CO;2.

Wobus, C., Whipple, K.X., Kirby, E., Snyder, N., Johnson, J., Spyropolou, K., Crosby, B., and Sheehan, D., 2006, Tectonics from topography: Procedures, promise, and pitfalls, *in* Willett, S.D., et al., eds., Tectonics, Climate, and Landscape Evolution: Geological Society of America Special Paper 398, Penrose Conference Series, p. 55–74, doi:10.1130/2006.2398(04).

Zerathe, S., Lebourg, T., Braucher, R., and Bourlès, D., 2014, Mid-Holocene cluster of large-scale landslides revealed in the southwestern Alps by ^{36}Cl dating. Insight on an Alpine-scale landslide activity: Quaternary Science Reviews, v. 90, p. 106–127, doi:10.1016/j.quascirev.2014.02.015.

Science Editor: Aaron J. Cavosie
Associate Editor: Frank J. Pazzaglia

Manuscript Received 24 May 2015
Revised Manuscript Received 29 December 2015
Manuscript Accepted 20 January 2016

Printed in the USA